Research Report 131
JANUARY, 1965

Internal Friction of H_2O, D_2O and Natural Glacier Ice

by

Daisuke Kuroiwa

U.S. ARMY MATERIEL COMMAND
COLD REGIONS RESEARCH & ENGINEERING LABORATORY
HANOVER, NEW HAMPSHIRE

SUMMARY

The three parts of this report are entitled (1) internal friction of pure H_2O, D_2O and doped ice crystals, (2) internal friction at crystal boundaries, and (3) the internal friction of natural glacier ice. Part 1 uses the flexural vibration method and expresses internal friction as a logarithmic decrement of free oscillation. Equations are given for the logarithmic decrement, internal friction, and the resonant frequency of a rectangular bar. In Part 2 the grain boundary internal friction of ice grown from a melt was measured by cutting blocks containing individual crystal boundaries from polycrystalline ice and inlaying these in single crystal bars. This friction depends upon concentrated chemical impurities. In Part 3 the internal friction of glacier ice was measured in specimens from Antarctica, Greenland, and Le Conte Glacier, Canada. Distinctively different curves were obtained for the specimens. These differences can be attributed to (1) environmental conditions at the time of formation, and (2) the environmental conditions that acted on the sample from the time of formation until the time of sampling.

CONTENTS

ILLUSTRATIONS

CONTENTS (Cont'd)

ILLUSTRATIONS (Cont'd)

INTERNAL FRICTION OF H_2O, D_2O AND NATURAL GLACIER ICE

Influence of Chemical Impurities on Mechanical Damping

by

Daisuke Kuroiwa

PART I. INTERNAL FRICTION OF PURE H_2O, D_2O AND DOPED ICE CRYSTALS

Introduction

When a solid bar is set into free vibration, the amplitude of its oscillations decreases with time. This is true even if the bar is completely isolated from its surroundings so that radiated sound loss and similar effects are negligible. This dissipation of vibrational energy is caused by internal friction. The internal friction (mechanical damping) of a solid bar is so structure-sensitive that it has been used as one of the fundamental methods of analyzing the internal structure of a crystalline solid in that damping can arise from crystal imperfections, such as lattice defects, chemical impurities, and inclusions.

When the measured internal friction (denoted as tan δ) of a crystalline solid can be expressed by the following relationship (Nakaya, 1959):

$$\tan \delta = (\tan \delta_{max}) \frac{2 \omega \tau}{1 + \omega^2 \tau^2} \qquad (1)$$

and

$$\tau = \tau_0 \exp \left(\frac{Q}{RT} \right), \qquad (2)$$

where ω is an angular frequency, τ is the relaxation time, Q is the activation energy, R is the gas constant, T is the absolute temperature, and τ_0 is a constant, one of the possible mechanisms of mechanical damping is simple atomic movement (diffusion) through the lattice defects.

The internal friction of ice has been measured by various authors using different techniques. Kneser et al. (1955) observed mechanical damping of a single ice crystal at temperatures ranging from 0C to -25C by means of torsional vibrations. They found that a single crystal of ice exhibits a typical mechanical relaxation phenomenon which can be expressed by eq 1 and 2. They obtained 8.5 Kcal/mole as a value for the activation energy. Kuroiwa and Yamaji (1956, 1959) used the flexural vibration method to measure the internal friction of both polycrystalline and single-crystal ice in a wide temperature range between 0C and -180C. They found that there are three kinds of mechanical damping produced by grain boundaries, proton movement, and chemical impurities. The observed activation energy due to proton movement was about 6 Kcal/mole. Recently, Schiller (1958) observed the mechanical relaxation of a pure single ice crystal by means of longitudinal and torsional vibrations. He found that the mechanical damping of a single ice crystal changed with crystallographic orientation and the mode of oscillation used. The observed activation energy was 13.4 Kcal/mole.

Ice crystals exhibit a remarkable mechanical relaxation phenomenon like that of "anelasticity" in metals. Although it is believed that mechanical relaxation in ice crystals is caused by proton movement by means of lattice defects, some discrepancies are found among the experimental data. The author believes that these discrepancies may be mainly attributed to the chemical impurities involved. The present study was undertaken in order to reveal how chemical impurities influence the mechanical damping of ice. First, pure H_2O and D_2O ice were studied to determine the temperature dependence of internal friction. Some differences in relaxation times due to the heavier mass of deutron were observed in D_2O ice. The main part of this paper is devoted to the investigation of doped ice crystals containing known chemical impurities such as NaCl, HCl,

NaOH, HF, NH_3, and NH_4F. The effect of grain boundaries on mechanical damping was clarified by a special technique which permitted measurement of the internal friction at the individual grain boundaries of polycrystalline ice. The internal friction at grain boundaries is not always proportional to the total area of the boundary, but is influenced by the chemical impurities concentrated in the boundary zone. These experimental data also provided an explanation for the characteristic mechanical damping curves observed in natural glacier ice.

Experimental Procedure

Internal friction, the rate of dissipation of energy, can be expressed by a logarithmic decrement of free oscillation. The amplitude of the free oscillation, in general, decreases exponentially with time. The amplitude of the damped oscillation is given by

$$A_n = A_0 \exp(-n\Lambda) \tag{3}$$

where A_0 is the initial amplitude, A_n is the nth amplitude counted from the time of initial damping, n is a positive integer, and Λ is a logarithmic decrement, expressed by

$$\Lambda = -\frac{1}{n} \ln \frac{A_n}{A_0}. \tag{4}$$

For small Λ, the relative dissipation of energy $\Delta W/W$ can be expressed by

$$\frac{\Delta W}{W} = \frac{A_{n-1}^2 - A_n^2}{A_n^2} = 1 - \exp(2\Lambda) = 2\Lambda. \tag{5}$$

where ΔW is the decrease of vibrational energy W per one cycle of oscillation. When a periodically varying stress is applied to a crystalline solid having internal friction, the relaxation then results in a strain that lags behind the stress. If we denote the periodical stress σ and the strain ϵ as

$$\sigma = \sigma_0 \exp(i\omega t) \quad \text{and} \quad \epsilon = \epsilon_0 \exp(i\omega t - \delta) \tag{6}$$

ΔW is calculated as follows:

$$\Delta W = \int_0^{\frac{2\pi}{\omega}} \sigma \frac{d\epsilon}{dt} dt = \pi \sigma_0 \epsilon_0 \sin\delta \tag{7}$$

where σ_0 and ϵ_0 are maximum stress and strain, ω the angular frequency, and δ the phase lag angle between applied stress and strain. Hence, the relative energy dissipation $\Delta W/W$ is

$$\frac{\Delta W}{W} = 2\pi \sin\delta = 2\pi \tan\delta \quad (\delta \ll 1). \tag{8}$$

From eq 5 and 8:

$$\tan\delta = \frac{\Lambda}{\pi}. \tag{9}$$

In our experiment, flexural vibration was used (Fig. 1). The vibration apparatus was placed in a cold box (A) which could be refrigerated with liquid oxygen or nitrogen. Rectangular ice bars P_1 and P_2, cut from the same ice block and trimmed to exactly the same dimensions, were cooled at the same rate. P_1 was used for temperature determination, and P_2 for mechanical damping. Thin iron bands I_1 and I_2 were attached to the ends of P_2. An exciting coil C_1 and a pick-up coil C_2 were placed about 5 mm below I_1 and I_2, respectively. P_1 and P_2 were suspended at their vibration nodal points by two fine silk threads stretched between the metal U-shaped brackets B. Alternating current was supplied to the coil through an audiofrequency oscillator. When the a-c frequency matched the proper vibrational frequency of P_2, resonance took place, and the induced current in the pick-up coil C_2 then reached a maximum value. The current in C_1 was short-circuited at this moment and the specimen P_2 began a damped free oscillation.

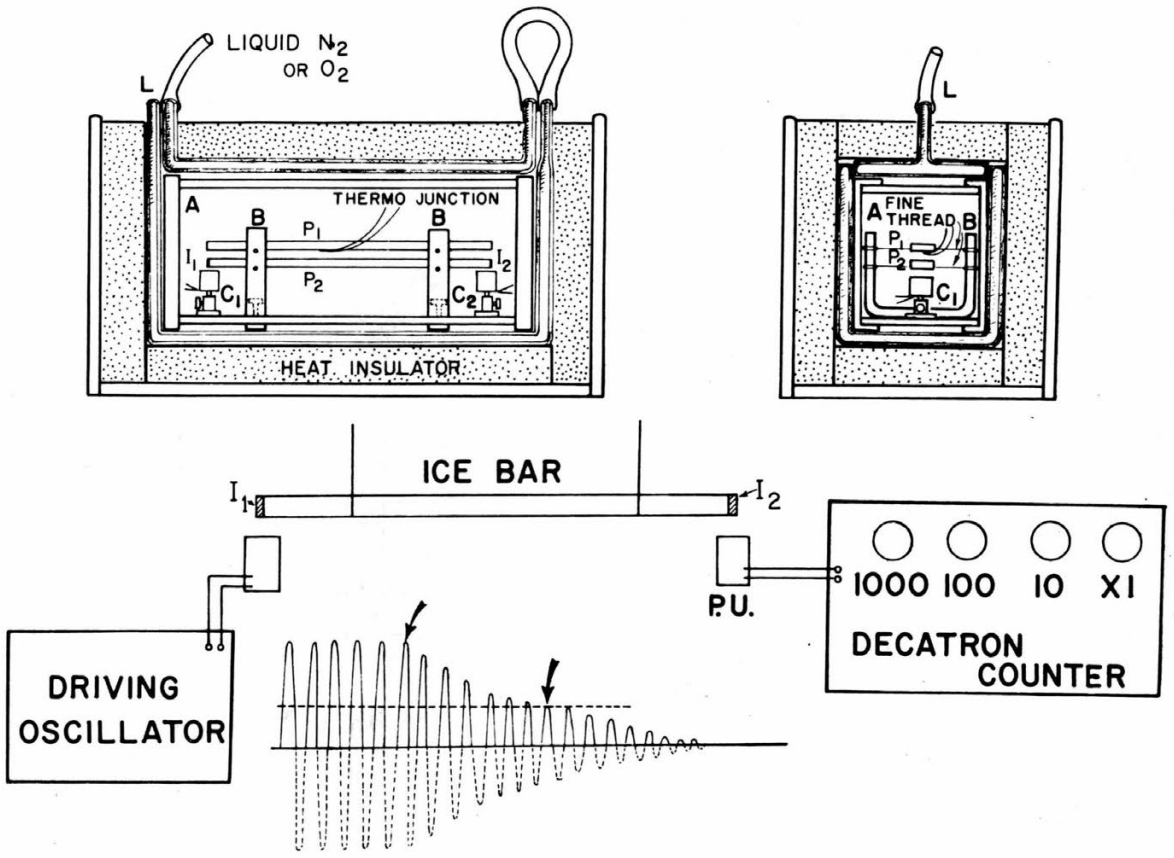

Figure 1. Vibration test apparatus.

The logarithmic decrement of the damped oscillation can be determined by counting the total number of oscillations N which occur while the amplitude (A) decreases to 1/nth of its initial value. If we take $A_n = (1/n)\, A_0$,

$$\Lambda = \frac{\ln n}{N} . \tag{10}$$

A special electronic device was designed to measure N. Figure 2 shows wiring diagrams of the audio oscillator (a) and the electronic counter (b). The induced voltage in the pick-up coil C_2 is transmitted to the "4-stage pulse counter" which consists of four electronic pulse-counter tubes (commercial name Decatron). A d-c ammeter M inserted in the pick-up circuit indicates the maximum amplitude at which resonance took place. A working voltage was previously set into the 6BN6 tube by adjusting the 20K rheostat, so that the Decatron counter will operate from the beginning of the damped oscillation until the amplitude (reading on M) drops to 1/nth of the initial value (operating period is between two arrows indicated in Figure 1). Since the Decatron tube records every peak oscillation, the total number N is indicated electrically on the Decatron tubes. S_1 (Fig. 2a) is a switch for short-circuiting the exciting current through coil C_1; S_2 (Fig. 2b) is a starting switch for the electronic counter. When the first grid of 6BN6 is grounded by S_2, the Decatron begins recording the number of the damped oscillations. Both S_1 and S_2 can be operated simultaneously by hand. Since the Decatron tubes can be zeroed electrically by operation of a "reset" switch S_3, it is easy to repeat the damping measurements.

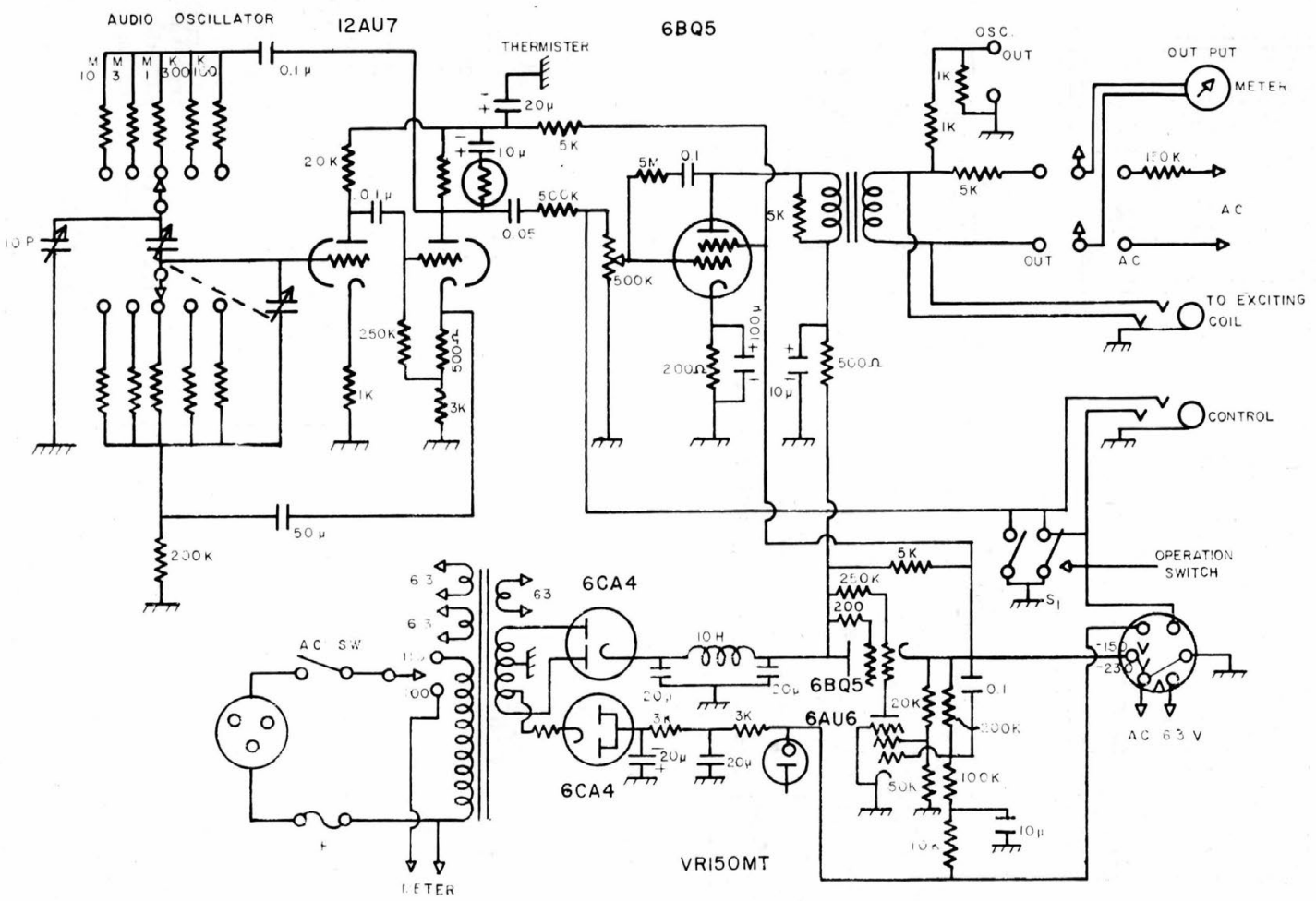

Figure 2a. Wiring diagram of the audio oscillator.

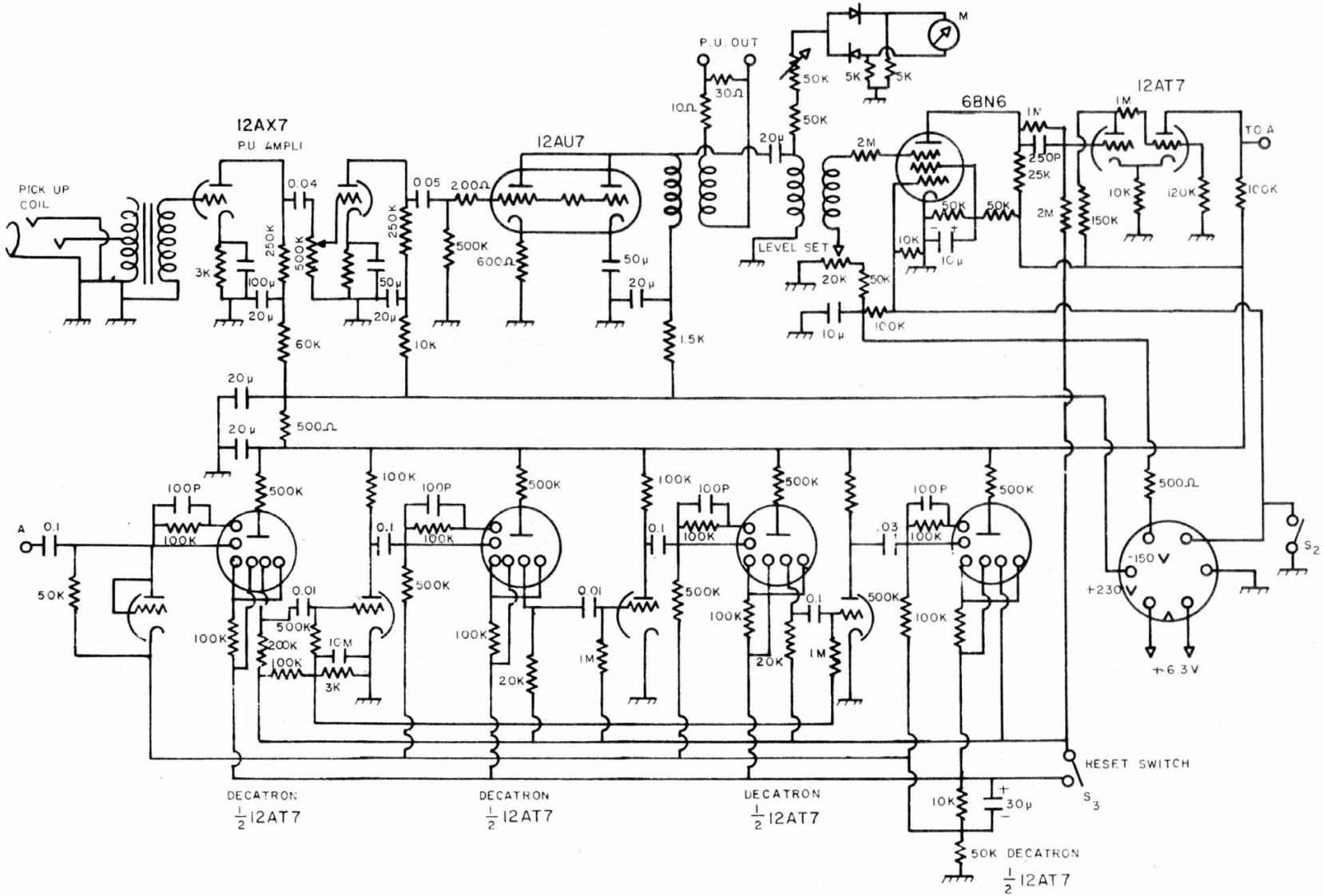

Figure 2b. Wiring diagram of the electronic counter.

The internal friction of all ice specimens was measured as a function of both temperature and frequency. The temperature of the specimen reached that of liquid nitrogen about 2 hours after the refrigerant was supplied into the cold box. The damping measurements were taken after stopping the coolant flow, and as the insulated box was slowly warming up.

According to the theory of flexural vibrations the resonant frequency of a rectangular bar is given by

$$f = \left\{ \frac{m^4 a^2 E}{48 \pi^2 \ell^4 \rho} \right\}^{\frac{1}{2}} \qquad (12)$$

where E is the elastic modulus, ℓ is the length of the specimen, a is its thickness, ρ is the density, and m is a constant determined by the mode of oscillation. The following numerical values of the constant m were used: 4.75 for the fundamental vibration, and 7.85 for the first overtone. It was difficult to change the resonant frequency over a wide range because of the limited size of the specimen.

Experimental Results

Temperature dependence of internal friction of pure H_2O and D_2O ice crystals

Pure H_2O ice was made by freezing distilled water, filtered through an ion-exchange resin, in a polyethylene container. A rectangular ice bar was cut from the transparent part of the frozen ice block. A microtome was used to trim the ice bar to precisely 196 mm long, 11.8 mm wide, and 3.7 mm thick. In order to eliminate the mechanical strain which could be created by the trimming, the specimen was put in a plastic envelope and kept at -10C for 1 or 2 days. A photograph of a specimen taken under polarized light is shown in Figure 3. The specimen consists of many large randomly oriented grains.

Figure 3. Grain structure of pure ice specimen photographed in polarized light. 196 mm long, 11.8 mm wide, 3.7 mm thick.

In Figure 4, curves 1 and 2 represent the typical temperature dependence of internal friction in pure ice measured at the fundamental mode, and its first overtone, respectively. These curves exhibit a remarkably sharp maximum damping. Resonant frequencies at maximum damping were 297 cps for the fundamental and 816 cps for the first overtone. Maximum damping occurred at -31.5C for the fundamental and -22C for the first overtone. Curve 3, the fundamental, and curve 4, the first overtone, show the mechanical relaxation for the same specimen after it was reduced to 2.4 mm thick and 11 mm wide. As frequency increased, the damping maxima shifted toward a higher temperature with a slight decrease in tan δ. In these experiments, the height of maximum damping of the pure H_2O ice occurred approximately between 0.0085 and 0.0095. The sharpness of the relaxation curves may be expressed as the width ΔT where tan δ is half the maximum. The mean value of ΔT is found to be about -25C. The slope of

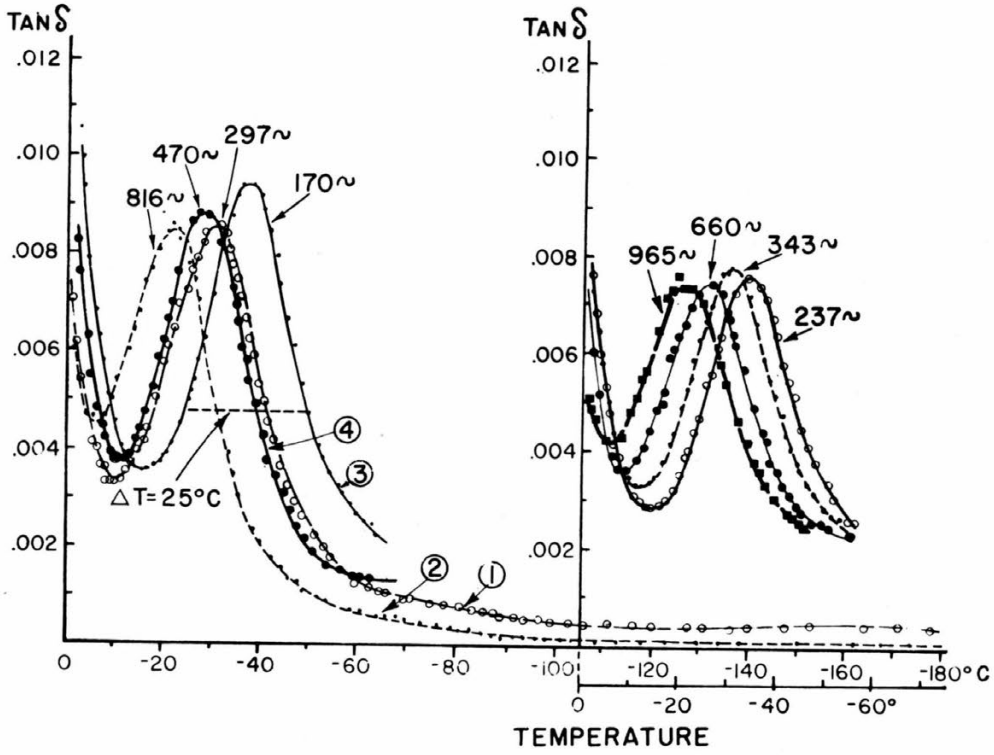

Figure 4. Typical temperature dependence of internal friction in pure H_2O ice.

Curves 1 and 2: Fundamental mode and first overtone, respectively, specimen 196 x 11.8 x 3.7 mm.
Curves 3 and 4: Fundamental mode and first overtone, respectively, specimen 196 x 11 x 2.4 mm.

the relaxation curves tended to extremely low values and no peculiarity was observed as the temperature was lowered to -190C. A steep rise of tan δ was found as the temperature approached the melting point. The deviation from the relaxation curve in the high temperature range is due to grain-boundary internal friction.

On the right side of Figure 4, the observed mechanical damping of another specimen of pure ice is illustrated as a function of temperature and frequency. Resonant frequency at maximum damping is indicated on each curve.

Electrical resistivity of a melted specimen, measured at room temperature, was used to determine the chemical impurity index. The electrical resistivity of the melted pure ice specimen was about 1300 Kohm · cm. Therefore, the electrical resistivity of doped ice can be expected to be much lower.

Liquid D_2O was frozen into a rectangular bar and prepared in the same manner as the H_2O block. The average grain size was similar to that of Figure 3. Figure 5 illustrates the typical temperature dependence of mechanical damping for D_2O ice. Damping maxima were observed between -10C and -40C, shifting toward higher temperatures with increased vibrational frequency. The resonant frequencies at the damping maxima are indicated on each curve. The measured temperatures for several of the curves were extended to -190C, but the slopes of the relaxation curves tended to the lower values and no peculiarity was found. In the high temperature range, however, the steep rise of tan δ caused by the boundaries appeared as the temperature approached the melting point. The average value for maximum damping and the sharpness of the relaxation curve are identical to those obtained for pure H_2O ice.

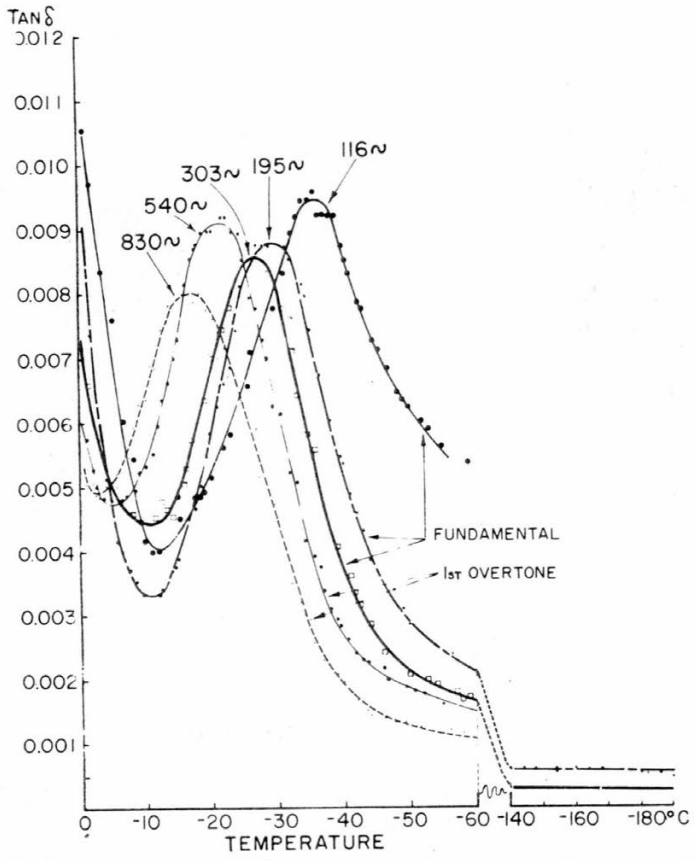

Figure 5. Typical temperature dependence of internal friction in pure D_2O ice.

Figure 6 represents the logarithmic relation of relaxation time τ and the reciprocal of absolute temperature T^{-1} at which the damping maxima appear. The relaxation time is given by the reciprocal of the angular frequency at which maximum damping occurs. The relationships for pure H_2O (open circles) and for D_2O (solid circles) ice are expressed well by Arrhenius's equation (eq 2).

The dielectric relaxation times measured by Auty-Cole (1952) in the same temperature range are also plotted for pure H_2O ice, and D_2O ice. They are also distributed well along each straight line, implying that mechanical and dielectrical relaxation processes originate by the same mechanism of proton movement. This observation is considered to be the most important outcome of the present work.

Gränicher et al. (1957) have explained the dielectric relaxation in pure ice in terms of dipole rotation through D- and L-defects, as suggested by Bjerrum (1952). In a perfect ice crystal, only one hydrogen atom lies on the line connecting two neighboring oxygen atoms. In non-perfect ice crystals, however, the 0-0 linkage may be occupied by two hydrogen atoms (D-defect) or none (L-defect). By rotation of a molecule adjacent to a D- or L-defect, the defect moves to a neighboring linkage and is thus able to diffuse in the crystal. The diffusion of these crystal imperfections causes reorientation of the protons and can lead to energy dissipation under the applied electric field.

The constant (pre-exponential factor) τ_0 and activation energy Q were found to be:

$\tau_0 = 6.9 \times 10^{-16}$ sec, $Q = 13.1$ Kcal/mole, for pure H_2O ice,
$\tau_0 = 1.04 \times 10^{-15}$ sec, $Q = 13.2$ Kcal/mole, for D_2O ice.

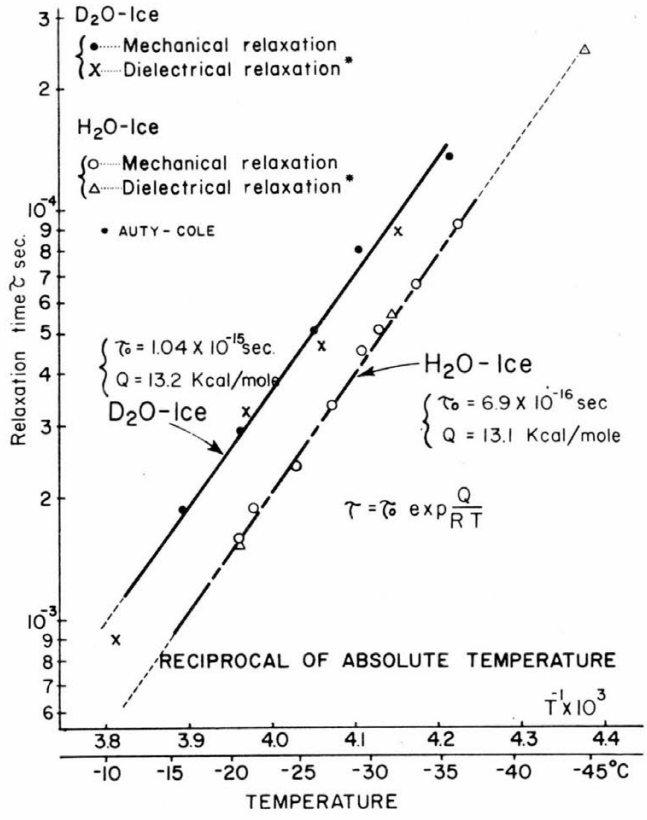

Figure 6. Relaxation time vs reciprocal of absolute temperature at maximum damping, pure ice.

Determining these numerical values always involves some error since they are obtained from the slope of the curve on a logarithmic scale. In our experiment, the resulting error can be considered to be about 5%. As shown in Figure 6, the observed relaxation time of D_2O ice is longer than that of the pure H_2O ice. The ratio of pre-exponential factors τ_0 (D_2O)/τ_0 (H_2O) is 1.5. This may be explained by the difference in mass between deutron and proton.

The good agreement of the observed damping curve with the theoretical curve is shown in Figure 7 (bottom). The theoretical curve was calculated from eq 1 and 2, using $\tau_0 = 6.9 \times 10^{-16}$ sec, Q = 13.1 Kcal/mole, tan δ_{max} = 0.0085, f = 297 cps. Deviations from the calculated curve are due to grain-boundary internal friction in the high temperature range and to radiated sound loss and loss of energy through the suspending threads in the low temperature range. The agreement of the curves indicates that the mechanical damping of ice is caused by a single relaxation mechanism. The deviation of the resonant frequency from the frequency at maximum damping is plotted versus temperature in the upper part of Figure 7. Resonant frequency dispersion and maximum damping took place in the same temperature range.

The dielectric loss (ε'') of a pure ice crystal measured by Smyth and Hitchcock (1932) is depicted as a function of temperature in the middle part of Figure 7. The temperature dependence of ε'' of pure ice is expressed by equations similar to eq 1 and 2. As shown in this figure, the maximum of dielectric loss shifts toward the high temperature range with an increase in frequency, and shows a slight decrease in the curve height. Comparison of the mechanical damping curve and the dielectric loss curve measured at 300 cps shows a similar temperature dependence and sharpness (ΔT = 25C).

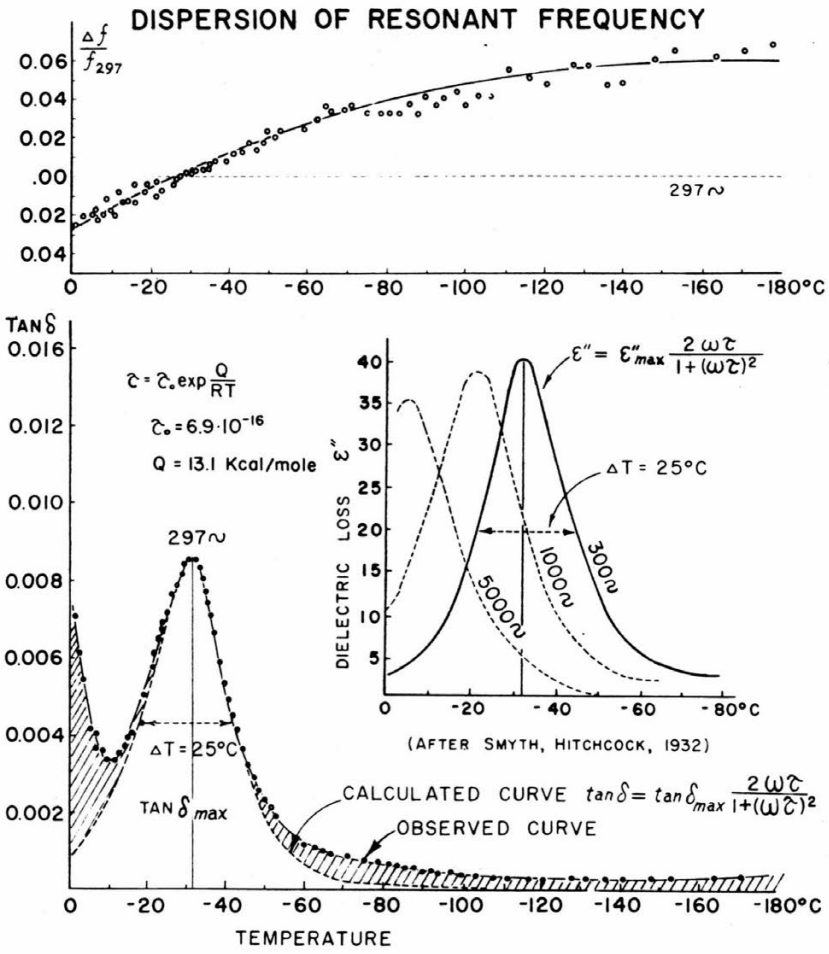

Figure 7. Observed and calculated damping curves for pure ice and dispersion of resonant frequency.

Influence of various chemical impurities on mechanical damping

Mechanical and dielectrical relaxation phenomena in ice crystals can be explained by proton movement through lattice defects. When doped ice is crystallized from water containing chemical impurities, some chemical additives may be captured. Since the lattice configuration near the captured impurities would be strongly modified, many lattice imperfections may be formed. The influence of chemical impurities on dielectric relaxation of ice has been studied by various authors, but a systematic investigation for mechanical relaxation has not yet been conducted. In the experimental investigations discussed here, NaCl, HCl, and NaOH were used as neutral, acidic, and alkaline additives which may behave as interstitial lattice modifiers. HF and NH_4F were used as substitutional lattice modifiers in the ice crystal.

Modification of mechanical damping due to NaCl, HCl, and NaOH. NaCl, a typical neutral compound, showed a modification of mechanical damping from the onset. A dilute aqueous solution containing 0.001 mole of NaCl was frozen in the cold room. A rectangular bar was cut from the doped ice block, and prepared in the same manner as before. The specimen consisted of large randomly oriented grains. The actual concentration of NaCl in the ice crystal was not measured, but the electrical resistivity for the melted specimen was 350 Kohm·cm, which is lower than the value for pure ice, indicating the existence of NaCl.

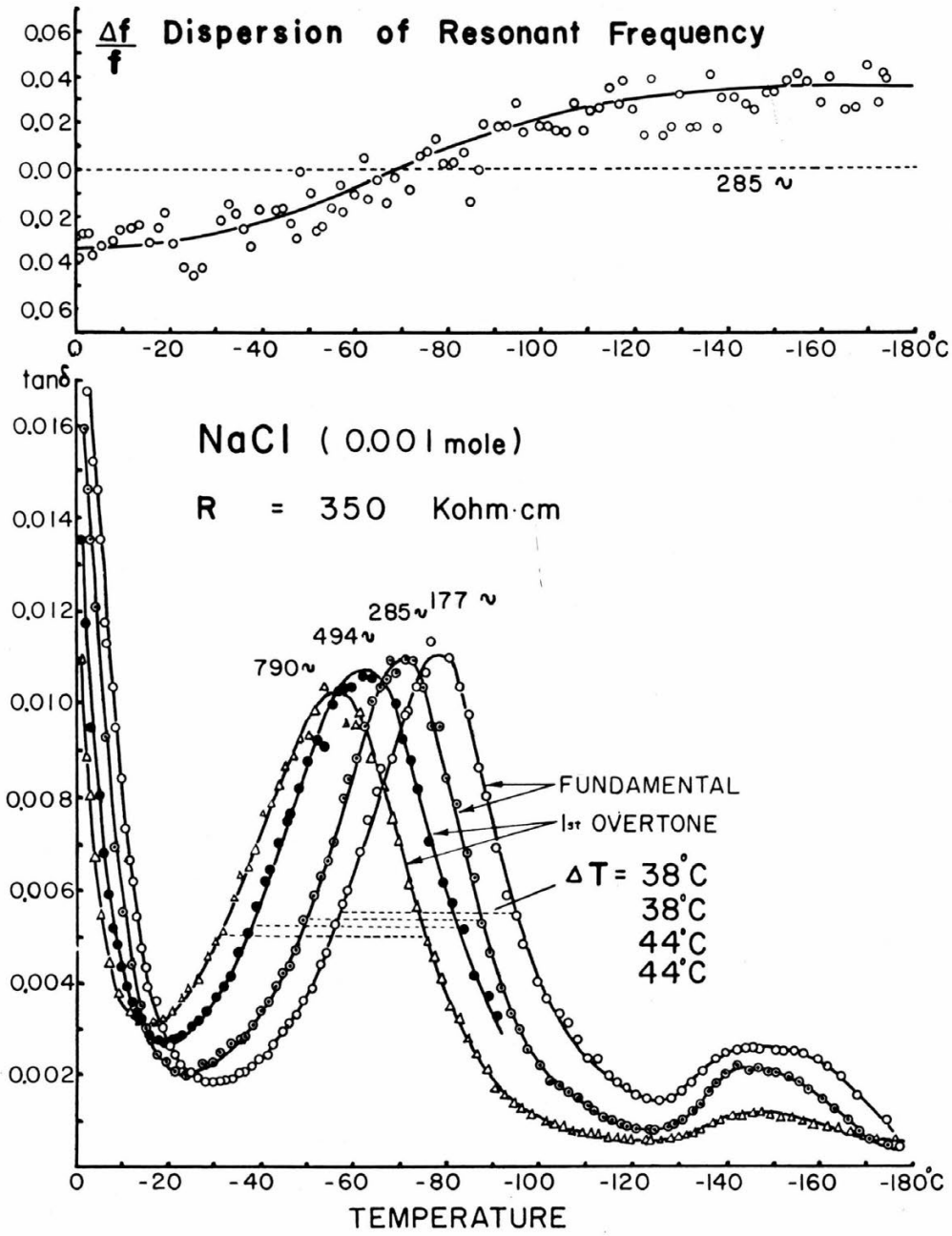

Figure 8. Temperature dependence of internal friction in NaCl ice.

Figure 8 depicts the effect of temperature variation on mechanical damping of NaCl ice. Several modifications were observed. The width ΔT of the relaxation curves due to proton diffusion became broader than that of pure H_2O ice, average ΔT = 41C at $\frac{1}{2}(\tan\delta)_{max}$. The damping maxima appeared in a lower temperature range than those of pure ice.

A new modification is the appearance of another damping maximum at around -145C. This low temperature damping was not observed in pure H_2O and D_2O ice. This maximum decreased inversely to vibrational frequency, but an appreciable

shift of its location was not observed. A steeper rise in grain-boundary internal friction appeared near the melting point. The dispersion of resonant frequency is shown in the upper part of Figure 8. The deviation of resonant frequency from f_{max} (285 cps) at which maximum damping occurs was plotted as a function of temperature. As shown by a solid curve, a steep variation of the resonant frequency occurs at the same intermediate temperature as maximum damping (lower figure) because of proton movement. No appreciable dispersion was observed in either high or low temperature ranges where tan δ rose steeply and another damping maximum appeared. The relation between relaxation time and the reciprocal of absolute temperature, both obtained from the resonant frequency and temperature at maximum damping, is plotted in Figure 9. From the slope of this curve, Q and τ_0 are found to be 5.57 Kcal/mole and 3.95×10^{-10} sec, respectively. These constants differ greatly from those of pure H_2O ice.

Figure 10 shows how the observed damping curve for NaCl-doped ice differs from a theoretical curve given by eq 1 and 2. The theoretical curve was calculated using the following numerical values: $\tau_0 = 3.9 \times 10^{-10}$ sec, $Q = 5.75$ Kcal/mole, $\tan \delta_{max} = \Delta_m = 0.011$, and $f = 285$ cps. As shown in this figure, the maximum damping curve for NaCl ice agrees with the calculated curve, suggesting that a simple relaxation-time theory is adequate to account for the experimental data obtained for NaCl-doped ice. Careful attention should be given to deviations (shaded area) in both high and low temperature ranges. Compare Figure 10 with Figure 7. One can easily recognize that grain-boundary internal friction increased remarkably in NaCl-doped ice crystals, and a new damping maximum appeared in the low temperature range.

An acidic-doped ice crystal was made by freezing a dilute acid solution containing 0.002 mole of HCl. A rectangular ice bar (190 mm long, 17.1 mm wide, 4 mm thick) was prepared from this ice block. The electrical resistivity of the melted specimen was 300 Kohm · cm. Figure 11 represents the temperature dependence of the

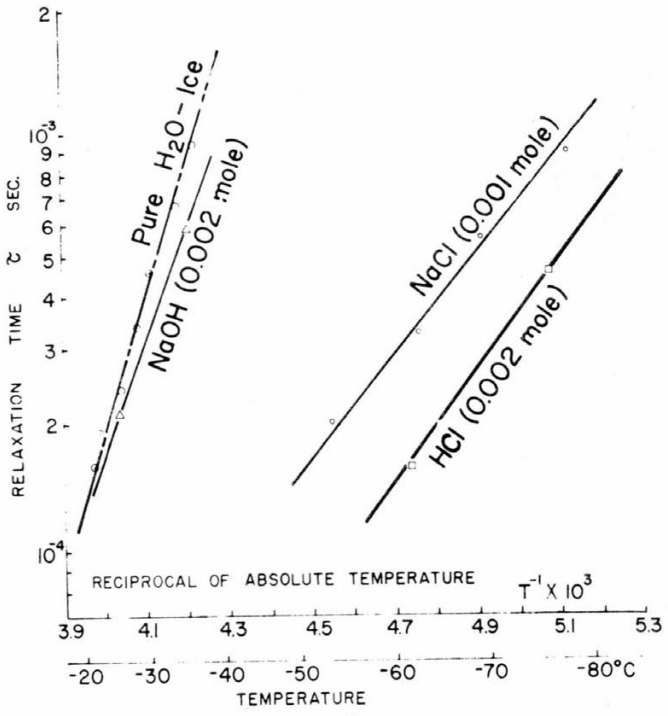

Figure 9. Relaxation time vs reciprocal of absolute temperature at maximum damping.

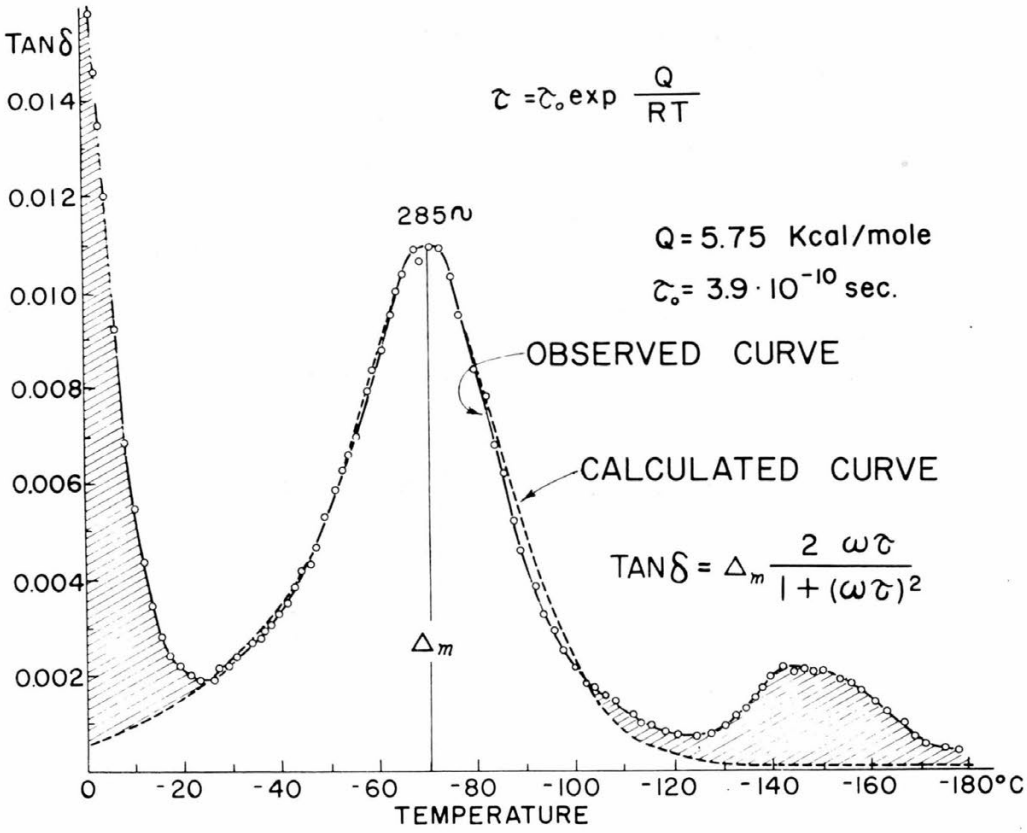

Figure 10. Observed and calculated damping curves for NaCl ice.

mechanical damping of Hcl ice measured at the fundamental and at the first harmonic vibrations. Modification of mechanical damping due to HCl was the same as that caused by NaCl. The relaxation curve due to proton movement became broad (mean ΔT = 40C). The steep rise of tan δ and mound-like damping appeared at high and low temperature ranges, respectively. The height of the mound-like damping decreased with frequency, but no temperature shift was observed. The relation between logarithmic plots of the relaxation time and the reciprocal of absolute temperature for maximum damping (see Fig. 9) give Q = 6.0 Kcal/mole, $\tau_0 = 8.95 \times 10^{-10}$ sec.

More complicated modifications of mechanical damping were observed in an alkaline-doped ice crystal (Fig. 12). This specimen was prepared from an NaOH solution, concentration 0.002 mole, with an electrical resistivity of 900 Kohm·cm when melted. The sharp relaxation curves, ΔT = 25C, appeared in the same temperature range as for pure H_2O ice. A peculiar damping curve was observed in the low temperature ranges, but its height decreased remarkably with frequency. The log τ vs T^{-1} for NaOH ice is illustrated in Figure 9. A straight line for this specimen is located at nearly the same temperature range as pure ice, showing that Q = 11.6 Kcal/mole, $\tau_0 = 1.2 \times 10^{-14}$ sec.

Impurity distribution in NaCl, HCl- and NaOH-doped ice crystals. Experimentation revealed that mechanical damping of ice can be modified by NaCl, HCl, and NaOH. If we assume that vibrational energy is dissipated only at the site of crystal imperfections and that a close correlation exists between impurity additives and defects, the following inferences can be drawn.

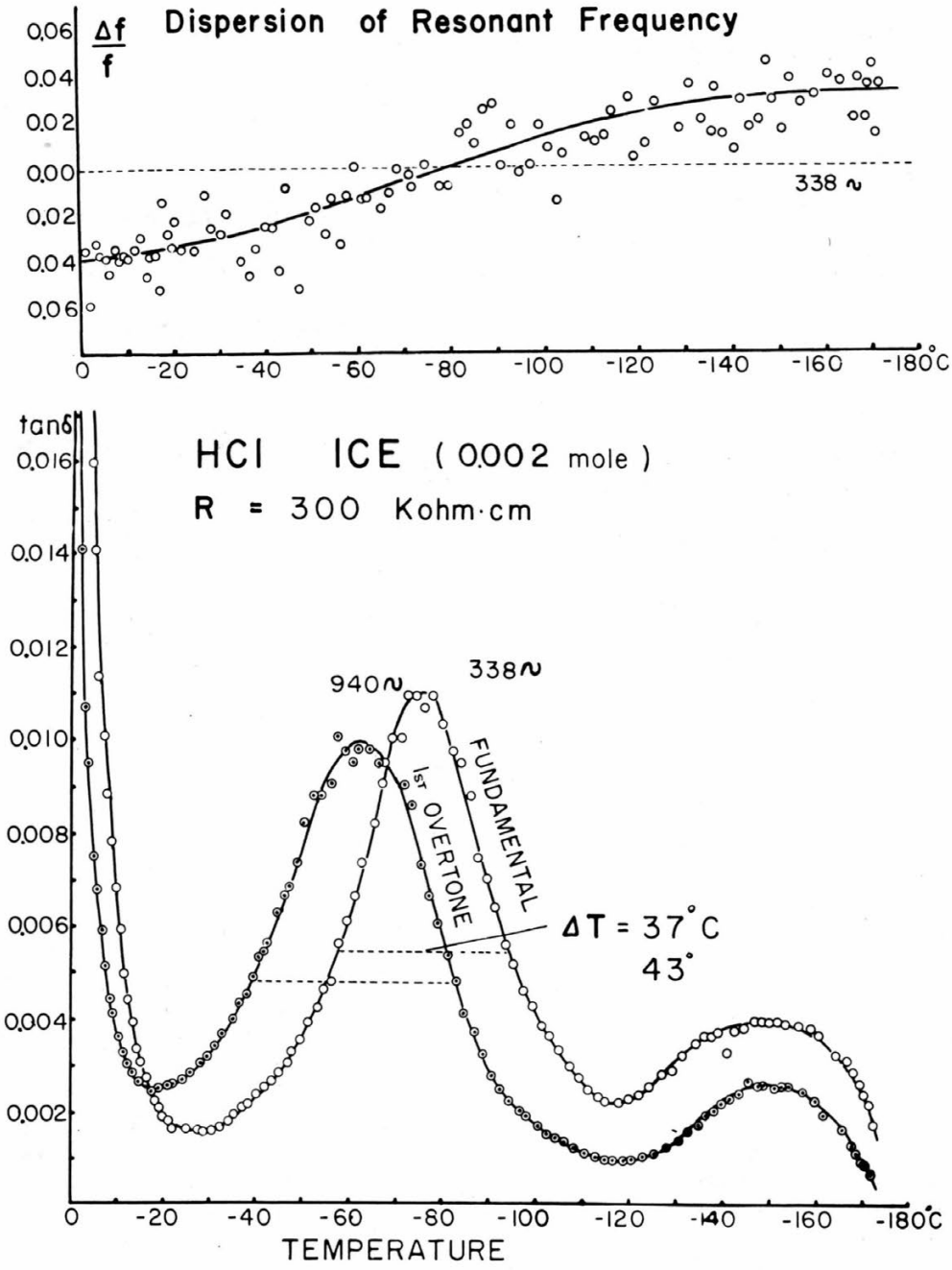

Figure 11. Temperature dependence of internal friction in HCl ice.

When a crystal grows from a melt or solution, it is believed that most of the impurities concentrate at the crystal boundaries, but some of them can exist in an atomic or an aggregated state within the grains. These three types of impurity distribution may each have a distinctively different influence on the mechanical damping of a crystal. In both NaCl- and HCl-doped ice crystals, the relaxation curve due to proton movement became broad and lowering of the activation energy and shortening of the relaxation time occurred. The dispersion of resonant frequency can also be closely correlated with maximum damping due to proton movement.

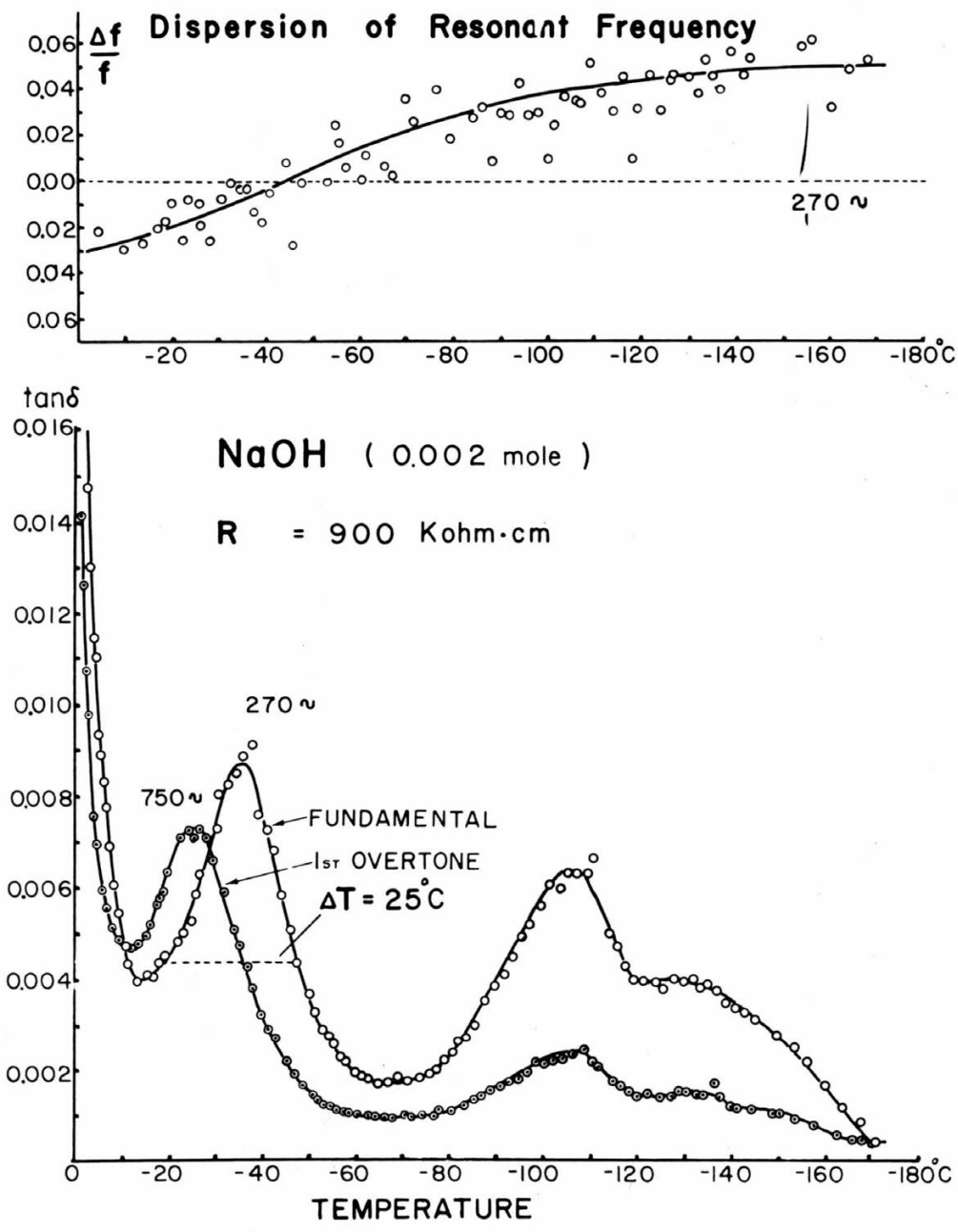

Figure 12. Temperature dependence of internal friction in NaOH ice.

According to Gränicher et al., the activation energy Q can be expressed as a sum of two components, Q_f (energy required for the formation of lattice defects) and Q_d (energy required for diffusion of defects). Gränicher et al. (1957) also suggested that $Q_f >> Q_d$. The lowering of the activation energy and the shortening of the relaxation time, therefore, may be caused by excess lattice defects created by the impurity additives. This suggests that NaCl or HCl can disperse homogeneously within the grains in an atomic or a molecular state similar to a solid solution and, consequently, may form more lattice defects than can be found in pure ice, thus strongly influencing mechanical

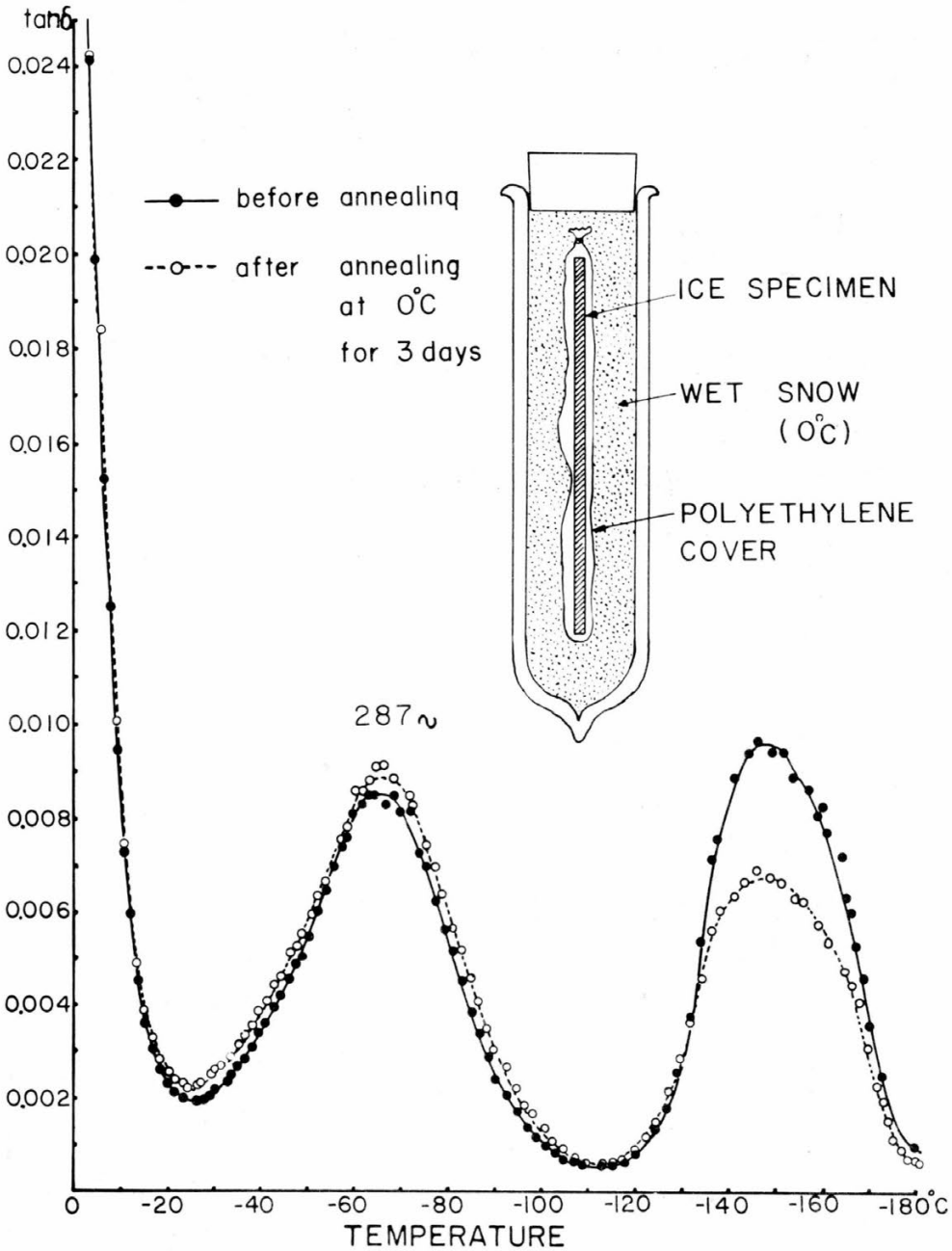

Figure 13. Effect of annealing on damping, commercial ice.

damping. Truby's (1952) experiment concerning the electrical properties of ice suggests that halogen ions incorporate substitutionally in the ice crystal lattice. It was difficult in our experiment, however, to determine whether NaCl or HCl exists either substitutionally or interstitially in the lattice.

The mound-like mechanical damping curve which appeared around -145C suggests that NaCl and HCl molecules can separate in aggregates at localized imperfections such as microscopic holes, pockets, or vacant places. This mound-like damping has never been observed in pure ice. The temperature range of this damping did not shift, though

its maximum value decreased with increasing frequency. Moreover, no dispersion in the resonant frequency occurred in the same temperature range as that of the mound-like damping. These observations indicate that the distribution and density of these imperfections may be localized in the ice crystal, and NaCl or HCl molecules may oscillate independently within such imperfections. Although a definite model for the microscopic holes or vacant places in an ice crystal lattice has not been proposed, experiments concerning the sintering of ice (Kingery, 1960; Kuroiwa, 1961) suggest the existence of this type of imperfection.

The third type of distribution is a concentration at the grain boundaries. At the front of a crystal growing in solution, an accumulation of impurities takes place. When two crystals grown from different nuclei meet, a large amount of impurities can be concentrated at the crystal boundary. Grain-boundary internal friction is caused by grain-boundary viscosity. (A detailed discussion is given in Part II.)

The most peculiar damping curve was observed in NaOH-doped ice. A sharp relaxation curve, ΔT = 25C, appeared, indicating that mechanical damping due to proton movement was not modified by the addition of NaOH. In fact a logarithmic plot of the relaxation time of this specimen is located in the same temperature range as pure ice (Fig. 9). The steep dispersion of resonant frequency was found only in the same temperature range as this maximum damping due to proton diffusion. The characteristic damping in the low temperature range, however, suggests that most NaOH molecules could be captured locally in aggregates.

The concentration of chemical impurities at localized crystal imperfections may depend upon: crystallization velocity, affinity for the H_2O molecule, and possibly other unknown variables. Their concentration, however, might be unstable in the ice crystal lattice.

The height of the mound-like damping around -145C can be reduced by annealing (Fig. 13). The specimen was prepared from ordinary commercial ice. The actual concentration of chemical impurities involved was not known, but the electrical resistivity was 450 Kohm·cm. The specimen shows a remarkable damping in the low temperature range. After the first measurement, the specimen was put in a polyethylene envelope and kept in a vacuum flask filled with wet snow (0C) for 3 days. After 3 days of annealing, noticeable decrease in height was observed in the low temperature damping, but no appreciable change was found in either the grain boundary or proton diffusion dampings.

The distribution of localized imperfections and defects along crystal boundaries can be changed by irradiation with heat rays (Fig. 14). A polycrystalline ice specimen was exposed to a strong infrared lamp for a few minutes, causing conspicuous internal melting at crystal boundaries and inside the grains. The low temperature mound-like damping greatly decreased after irradiation and grain-boundary internal friction increased remarkably, but no appreciable change was observed in the height of maximum damping due to proton movement. The process of internal melting due to irradiation is not completely understood. Nakaya (1956) suggested that Tyndall figures may be formed by colloidal particles or lattice defects absorbing the heat rays and consequently causing internal melting. It is quite natural to suppose that concentrated chemical impurities at localized imperfections would begin to melt when the temperature approaches the melting point, causing a change in the impurity distribution. During irradiation, some chemical impurities within the grains could diffuse to the grain boundaries, greatly influencing mechanical damping. Glacier ice usually contains chemical impurities, but it does not show any mound-like damping in the low temperature range. This also can be explained by the annealing effect which glacier ice is subjected to for long periods of time. A detailed discussion of this is given later.

Modification of mechanical damping as a function of NaCl concentration. Various ice specimens were made from aqueous solutions with NaCl concentrations of 0.005 mole to 0.00001 mole. The same volume of solution was frozen under the same cooling conditions. All specimens were trimmed to the same dimensions by means of a microtome, so that they could be measured at the same frequency.

Figure 15 illustrates typical variation of mechanical damping as a result of NaCl concentration. The resonant frequencies of the specimens were the same within

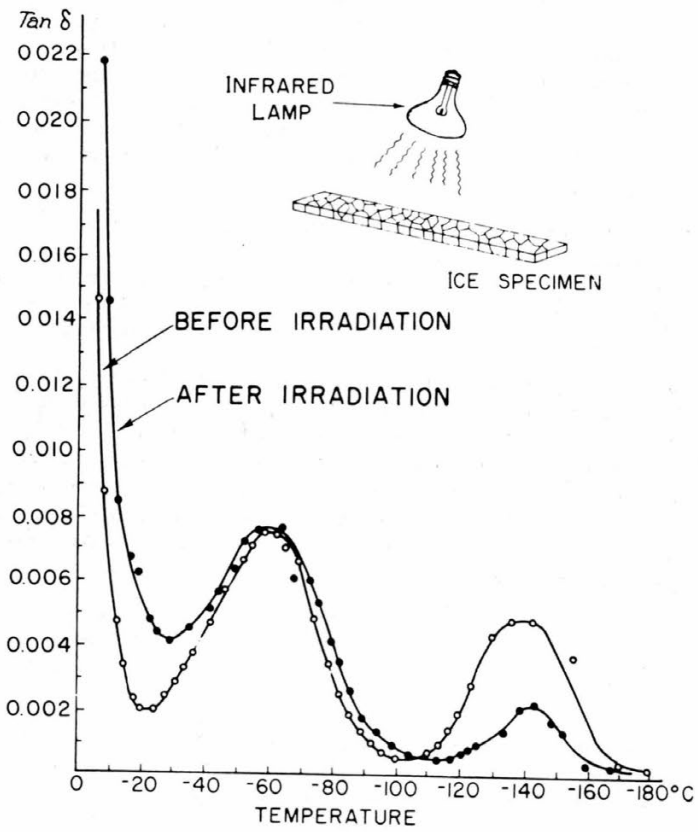

Figure 14. Effect of irradiation on damping, polycrystalline ice.

several percent. The relaxation curve of the specimen crystallized from the most dilute solution (0.00001 mole) was approximately the same as the curve for pure ice. Good superposition of the curves is seen in the same temperature range. The relaxation curve became broad (ΔT = 42C) at concentrations above 0.00005 mole, and maximum damping shifted toward the low temperature ranges with increase in concentration. The mound-like damping at low temperature was seen at higher concentration. The appearance of this damping may depend upon the concentration of the solution and the crystallization velocity of ice. Grain-boundary internal friction also increased with an increase in the NaCl concentration.

Figure 16 gives the logarithmic plots of relaxation time vs T^{-1} for various NaCl concentrations. The curve for the most dilute specimen (0.00001 mole) is in the same temperature range as pure ice, having the activation energy Q = 13.2 Kcal/mole. The slopes of the log τ vs T^{-1} curve are slightly less at concentrations > 0.00005 mole but are about the same. Consequently, the activation energies are all close to 6.6 Kcal/mole. The curve shifted toward the low temperature range with increased NaCl concentration.

Modification of mechanical damping due to HF and NH_4F. The fluoride ion has been regarded as one of the most favorable substances to make a solid solution with ice. Truby (1955), in his X-ray study of fluoride-doped ice crystals, found that a fluorine atom can occupy substitutionally the site of oxygen without any distortion of the ice unit cell. (The diameters of the fluorine and oxygen atoms are nearly the same.) Therefore, the manner in which mechanical damping is modified should depend upon whether the impurity atoms enter the ice crystal lattice interstitially or substitutionally. Two HF-doped ice crystals were made by freezing aqueous solutions containing 0.005 mole and 0.0025 mole of HF. The electrical resistivities of melted water from these specimens were 350 Kohm·cm and 500 Kohm·cm, respectively.

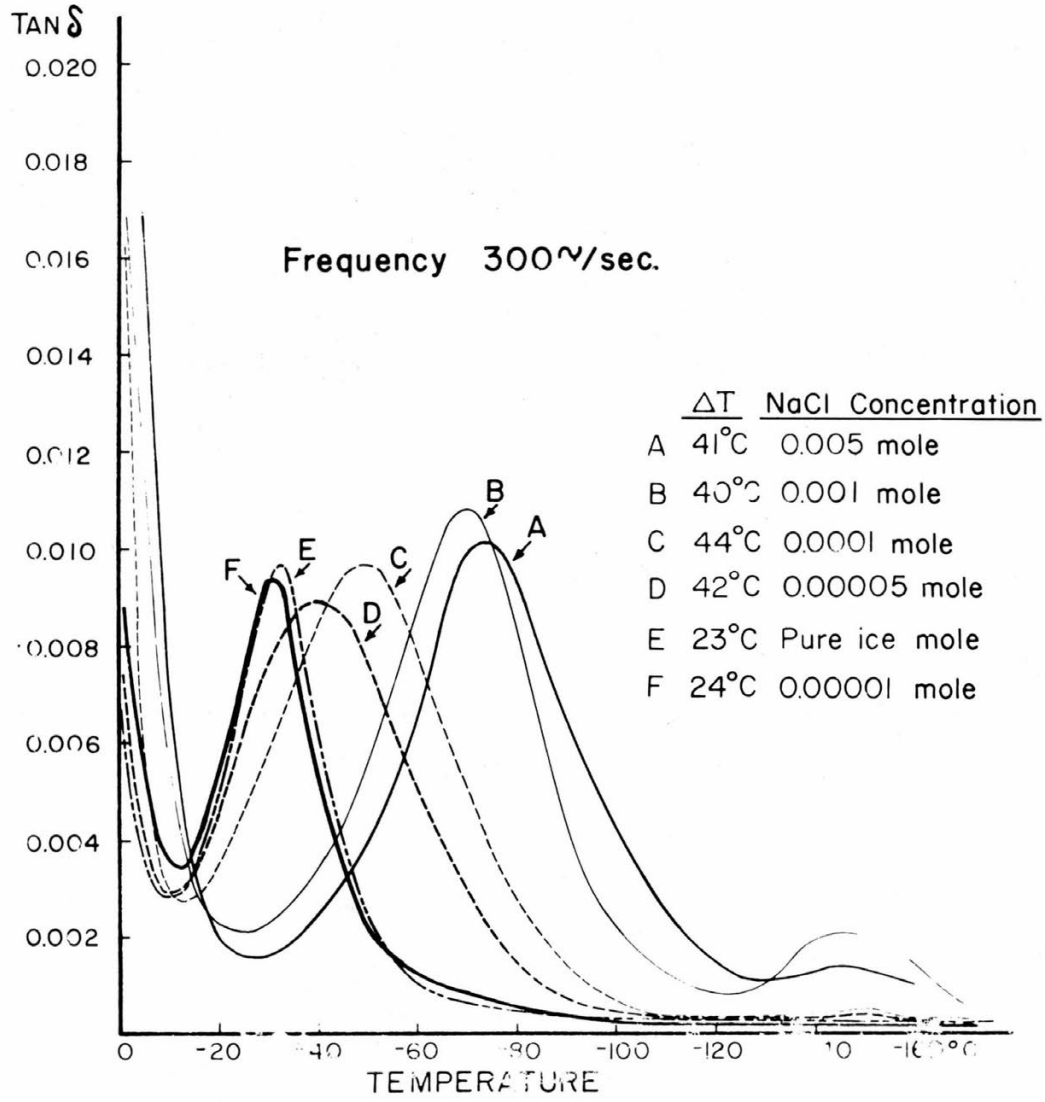

Figure 15. Typical variation of mechanical damping with NaCl concentration.

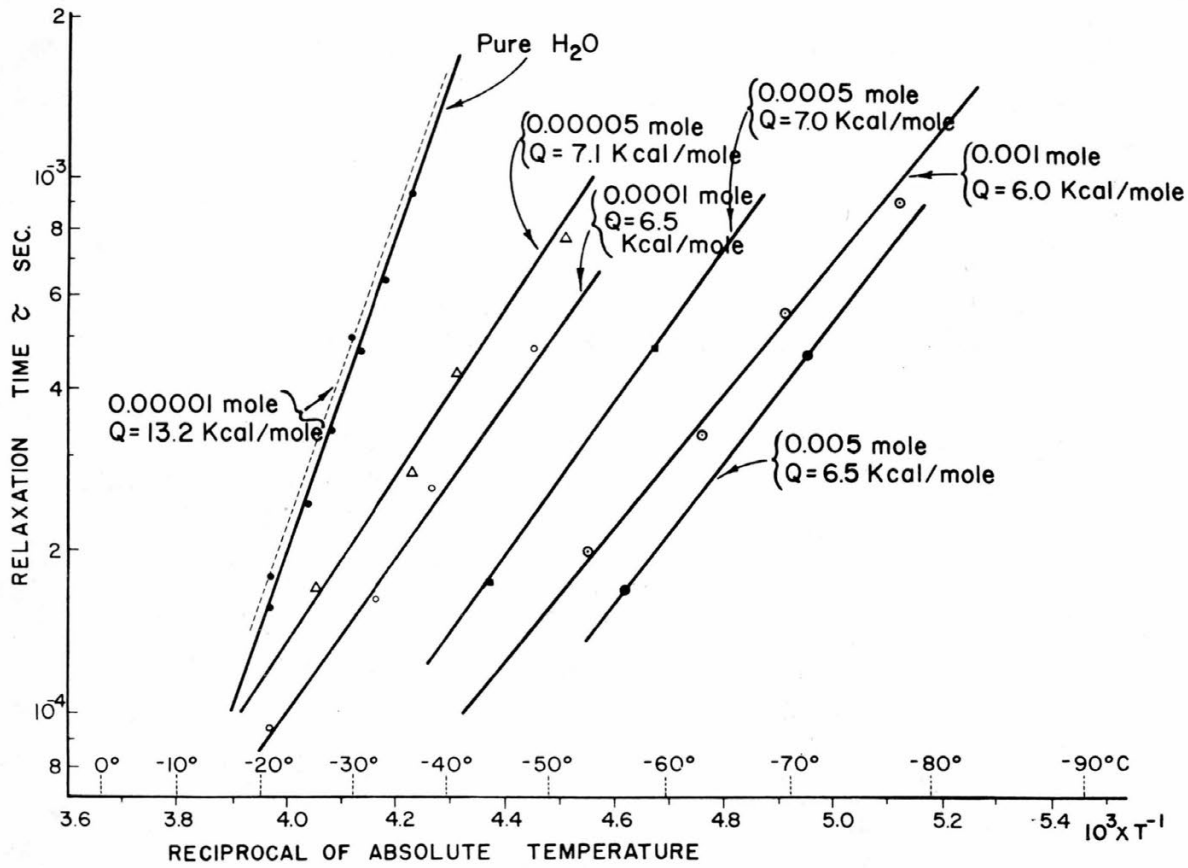

Figure 16. Log τ vs T^{-1}, ice with various NaCl concentrations.

Figure 17 illustrates the temperature dependence of the mechanical damping of HF ice obtained from a 0.005-mole solution. The two solid curves represent observed data for the fundamental and first harmonic vibrations. The relaxation curves become broad (mean ΔT = 41C), and result in a reduced activation energy (Q = 5.6 Kcal/mole) for the proton movement. No peculiar damping, however, was observed in the low temperature range as seen in NaCl- or HCl-doped ice crystals. Since the fluorine atom can occupy the lattice site of the oxygen, the following reaction might be established in HF-doped ice crystals.

$$HF + H_2O \rightleftharpoons F^- + H_3O^+$$

The observed modification of the relaxation curve, therefore, could be caused by the H_3O^+ ions produced by the addition of HF. Noticeable shift of the relaxation curve toward the high temperature range and reduction of maximum height was observed after this specimen was kept at -3.0C for 10 days.

In Figure 18, curve a shows the logarithmic plot of the relaxation time of this specimen against T^{-1}. From the slope of curve a, we obtain Q = 5.6 Kcal/mole, τ_0 = 1.05 $(10)^{-10}$ sec. After annealing at -3.0C for 10 days, curve a shifted to b. Curve c represents log τ vs T^{-1} for the specimen produced from the solution containing 0.0025 mole HF.

A poor agreement was found between the observed damping curve and the theoretical curve (Fig. 19) calculated from eq 1 and 2, using the following numerical values: Q = 5.6 Kcal/mole, τ_0 = 1.05$(10)^{-10}$ sec, Δ_m = tan δ_{max} = 0.0095, and f = 340 cps. The deviation (shaded area) from the theoretical curve means that the single relaxation time theory is inadequate to account for the experimental data of HF-doped ice.

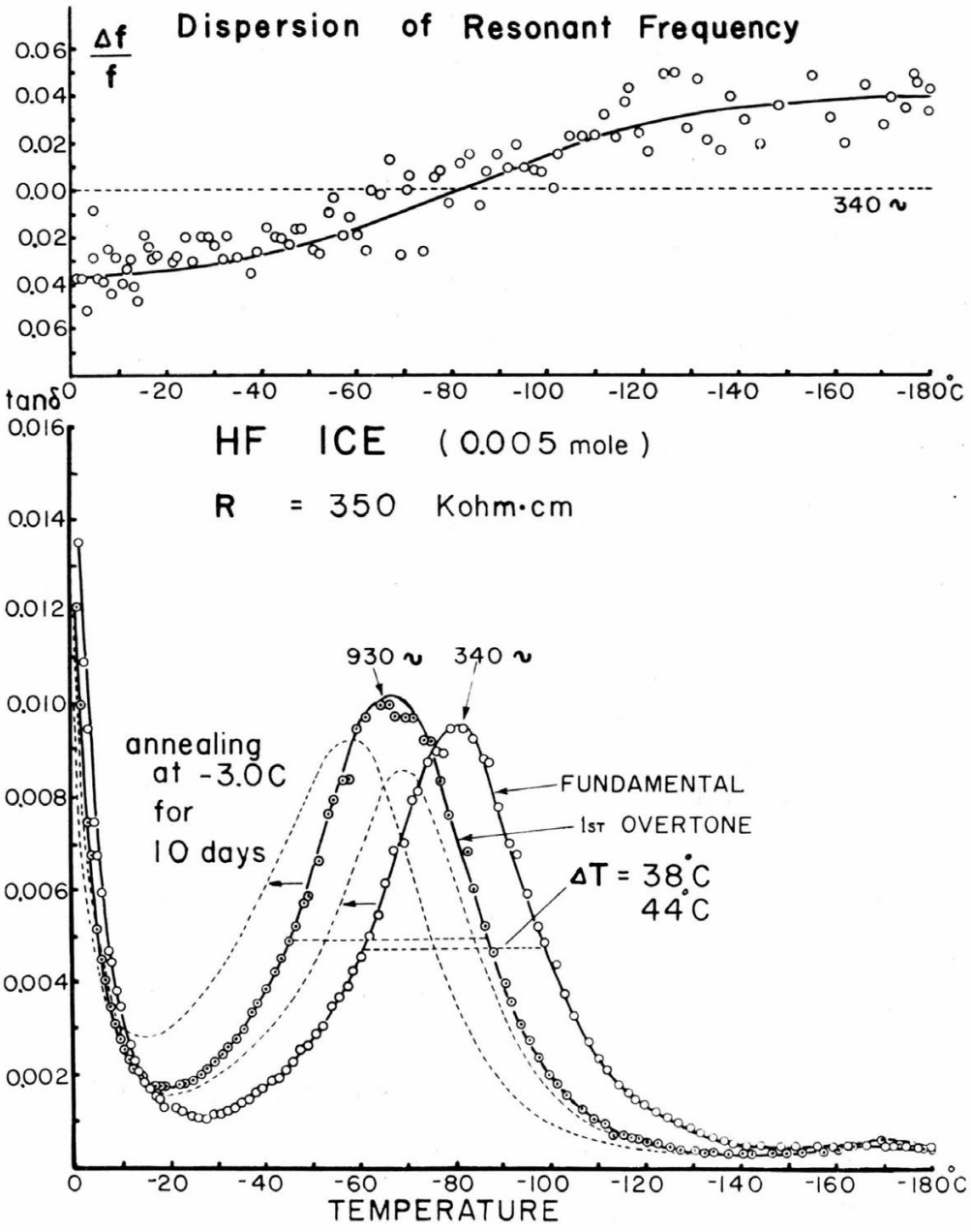

Figure 17. Temperature dependence of internal friction in HF ice.

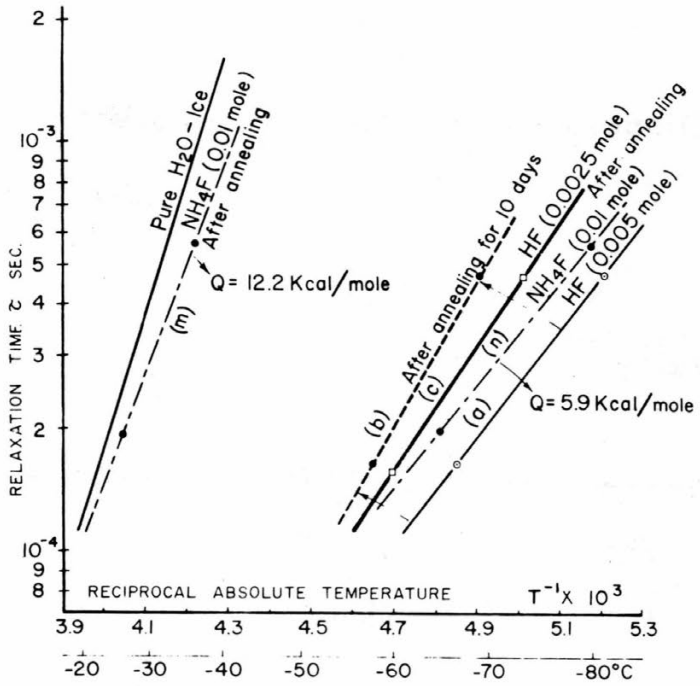

Figure 18. Log τ vs T^{-1}, HF ice and NH_4F ice.

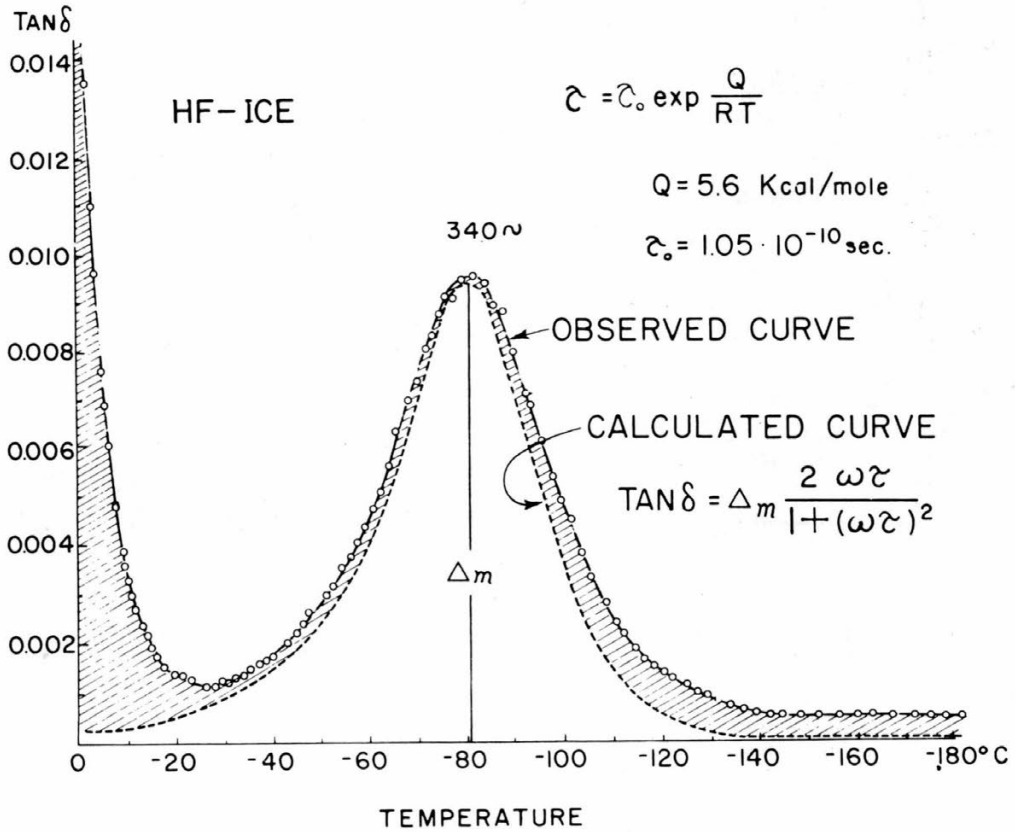

Figure 19. Observed and calculated damping curves for HF ice.

Conspicuous modification and an annealing effect on the mechanical damping curve was also observed in the NH_4F-doped ice crystals. The specimen was made from an aqueous solution containing 0.01 mole NH_4F. The electrical resistivity of this melted specimen was only 3 Kohm·cm. The relaxation curve (Fig. 20A) was very broad (ΔT = 88C) and maximum damping was difficult to determine. Dispersion of resonant frequency took place throughout the entire temperature range. After the first measurement, this specimen was put in a polyethylene envelope and annealed at -3.0C. After 7 days of annealing (Fig. 20B), a noticeable maximum appeared on each curve, reducing the height of damping on the low temperature side. After 23 days (Fig. 20C), two distinguishable maxima were observed on the damping curve as indicated by m and n, and the location of both maxima shifted toward a higher temperature range with increased frequency.

The log τ vs T^{-1} curves obtained for both m and n maxima are plotted in Figure 18. Curve m is located in nearly the same temperature range as pure ice with a steep slope Q = 12.2 Kcal/mole. The appearance of the two separate maxima in the relaxation curve can be ascribed to the internal change in chemical composition of the specimens. It is supposed that many relaxation mechanisms having different relaxation times existed in this sample when it was prepared from an ice block immediately after freezing and that unstable mechanisms having higher free energy were eliminated gradually by annealing, which can form nearly impurity-free regions within ice crystals.

According to Brill and Camp (1961), NH_4F may decompose in solid solution to the following two components.

$$2\ NH_4F \rightarrow NH_3 + NH_4 \cdot HF_2$$

NH_3 generated by this decomposition may be in a gaseous state. Since occlusion of gaseous ammonia in ice is very difficult, it may be diffused out from the inside of grains to the crystal surfaces, leaving an NH_3-free zone. The impossibility of the occlusion of NH_3 in ice is easily demonstrated by freezing an ammonia solution. An aqueous solution containing 0.005 mole of NH_3 was frozen, and a specimen was prepared. The internal friction was measured at both fundamental (312 cps) and first overtone (865 cps) vibrations. Sharp relaxation curves were observed in the same temperature range as pure ice, showing that ΔT = 23C and the activation energy Q = 12.5 Kcal/mole. No peculiar damping was observed in the low temperature range. In fact, the electrical resistivity of this melted specimen was found to be 1200 Kohm·cm (approximately the same as pure ice crystals), implying that the occlusion of ammonia is difficult even at the grain boundaries. It can be concluded that long annealing of NH_4F ice near the melting point results in the separation of nearly pure crystals from doped crystal regions indicated by m and n in Figure 20C.

Minimum concentration of NH_4F which can modify an ice crystal lattice. The minimum concentration of NaCl which was found to influence mechanical damping was between 10^{-5} mole and $5(10)^{-5}$ mole (in ice) as shown in Figure 16. In substitutional impurities, however, modification of the relaxation curve may be observed at very much lower concentrations. Ice specimens were made by freezing various dilute solutions of NH_4F. The specimen made by freezing a 10^{-7} mole NH_4F solution showed relaxation curves similar to those of pure ice (ΔT = 24C). When the concentration of NH_4F was increased to $5(10)^{-7}$ mole, an obvious change was observed on the low temperature side of the relaxation curves. The measured frequencies for the fundamental and first harmonic vibrations are indicated on each curve. At higher concentrations, above 10^{-4} mole, it was difficult to determine precisely the location of maximum internal friction because of the broadness of the damping curve. As shown in Figure 21, log τ - T^{-1} curves shifted toward the low temperature side with increased concentration, and the accompanying decrease in slope indicates a decreased activation energy. Similar phenomena have been observed in the dielectric properties of solid solutions of ice and NH_4F by Zaromb and Brill (1956). The minimum concentration of NH_4F having a significant influence on mechanical damping must be between 10^{-7} mole and $5(10)^{-7}$ mole (in ice). Therefore NH_4F can modify the ice lattice structure even at extremely low concentrations.

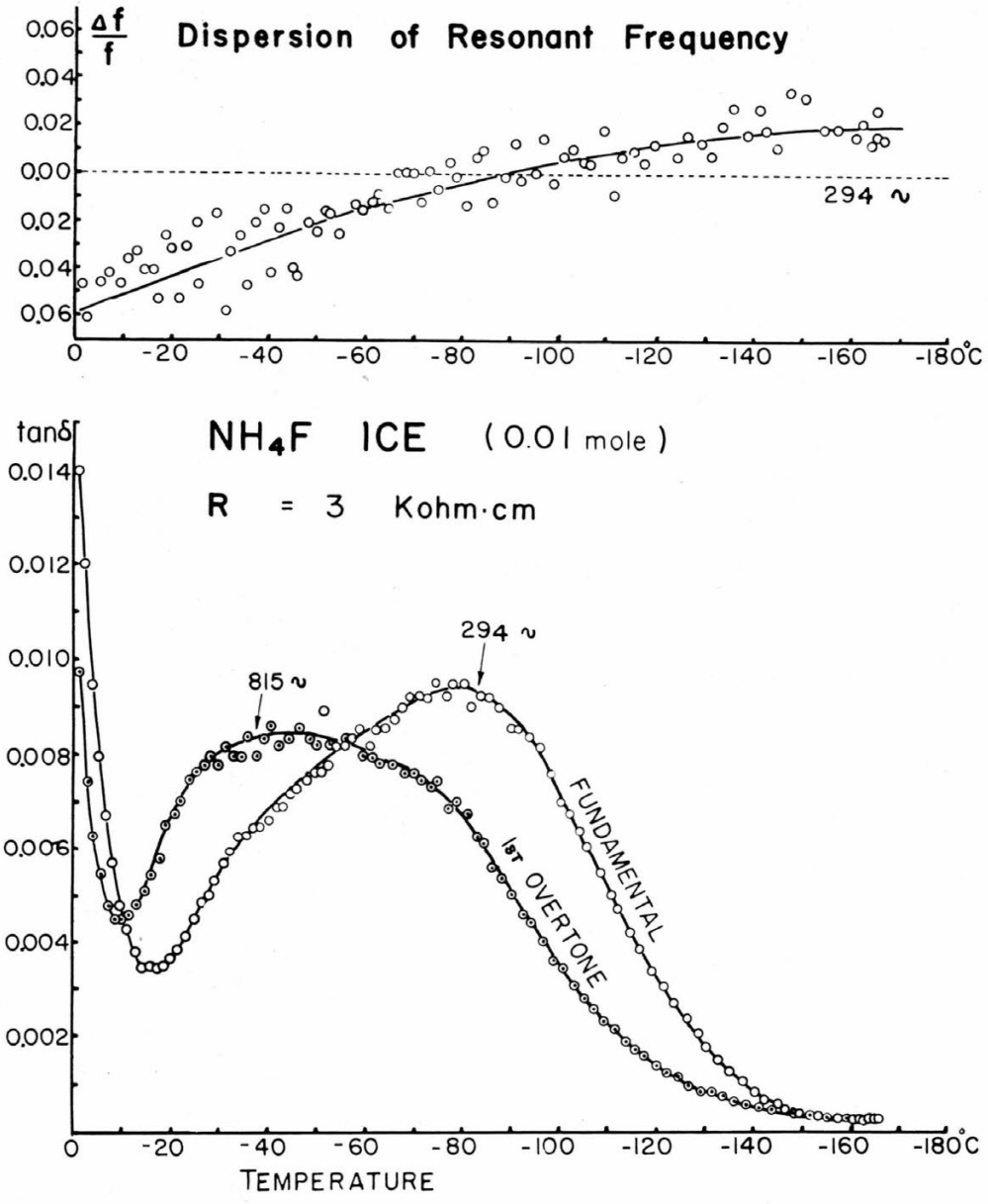

A.

Figure 20. Temperature dependence of internal friction in NH_4F ice.

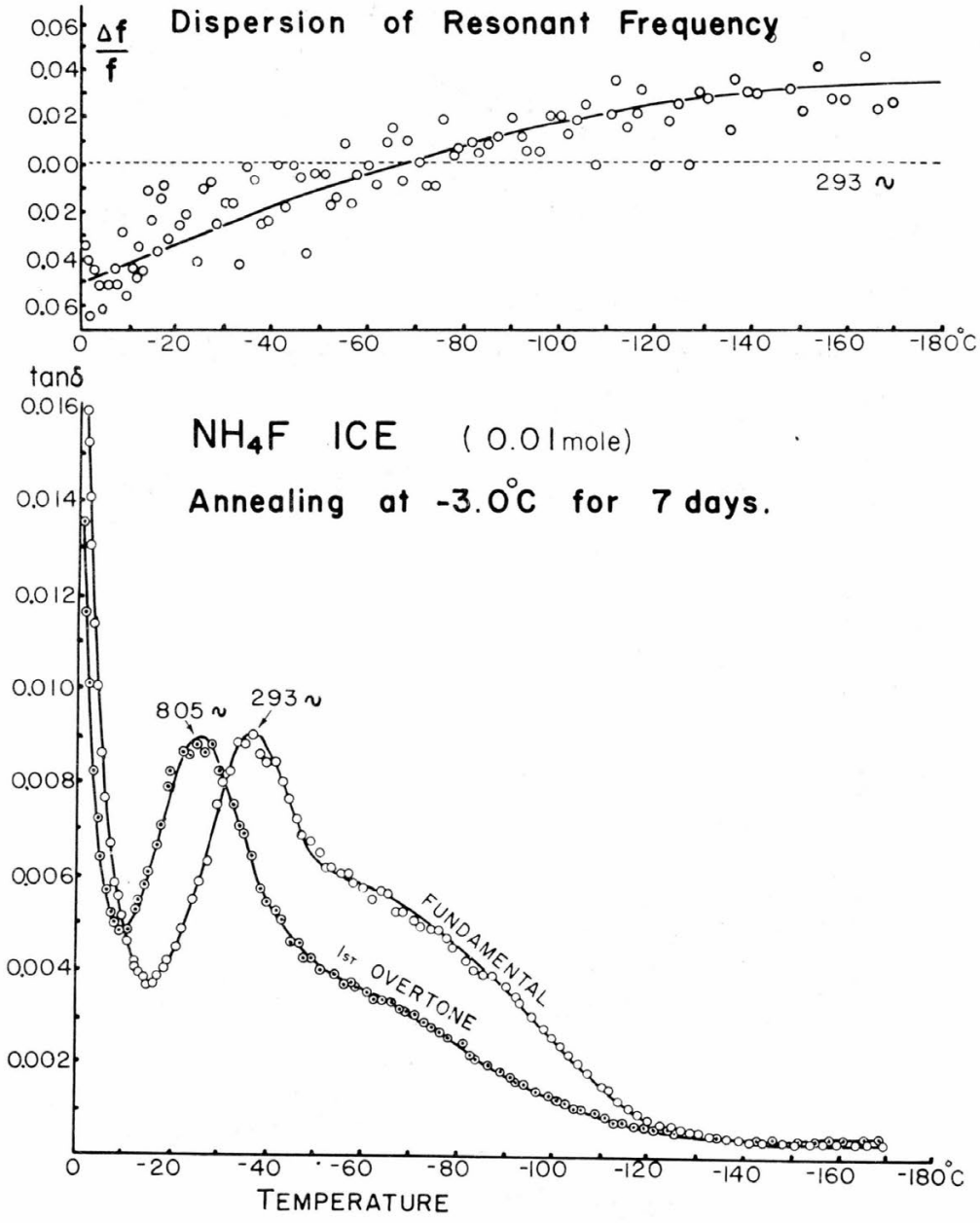

B.

Figure 20. (Cont'd) Temperature dependence of internal friction in NH_4F ice.

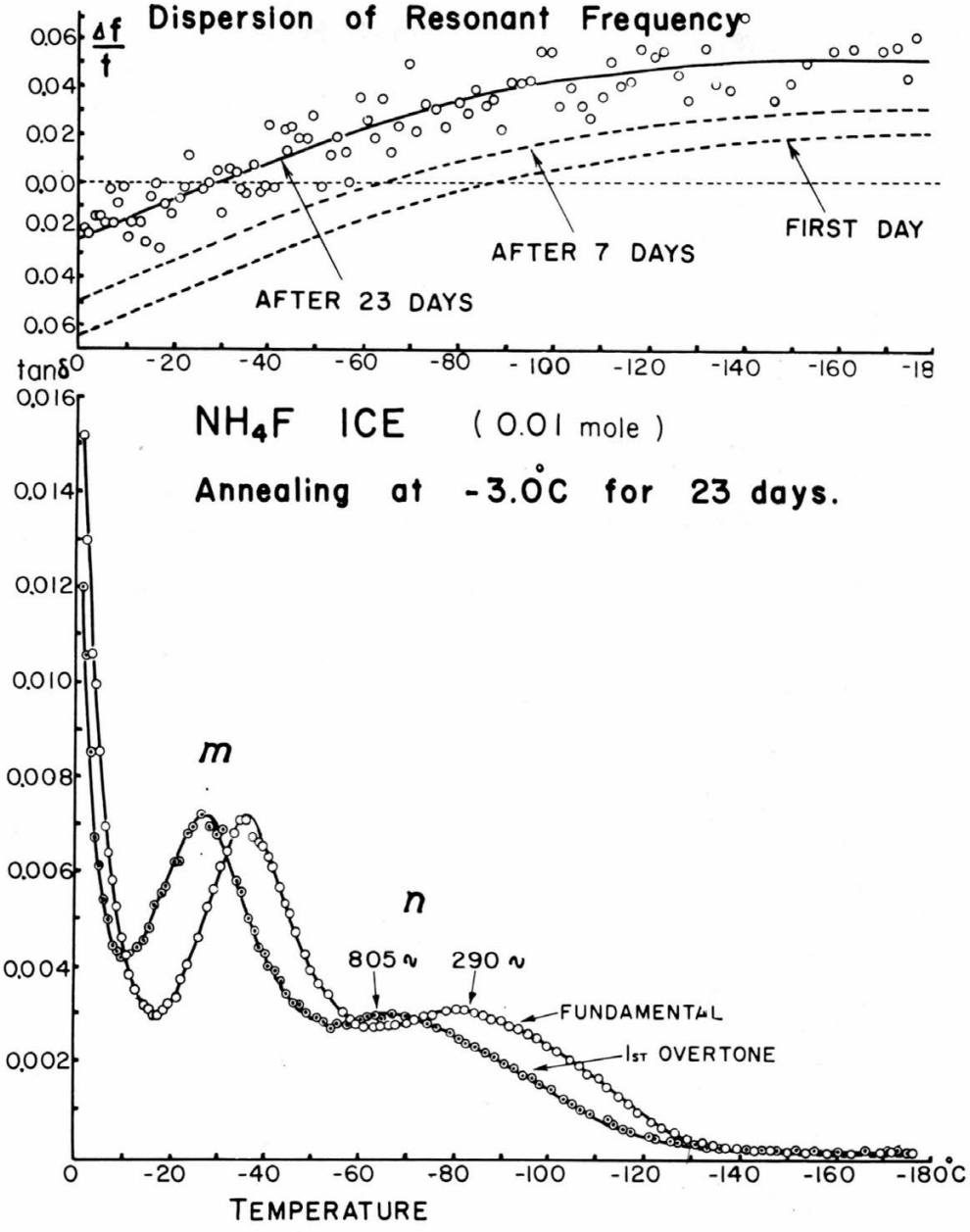

C.

Figure 20. (Cont'd) Temperature dependence of internal friction in NH_4F ice.

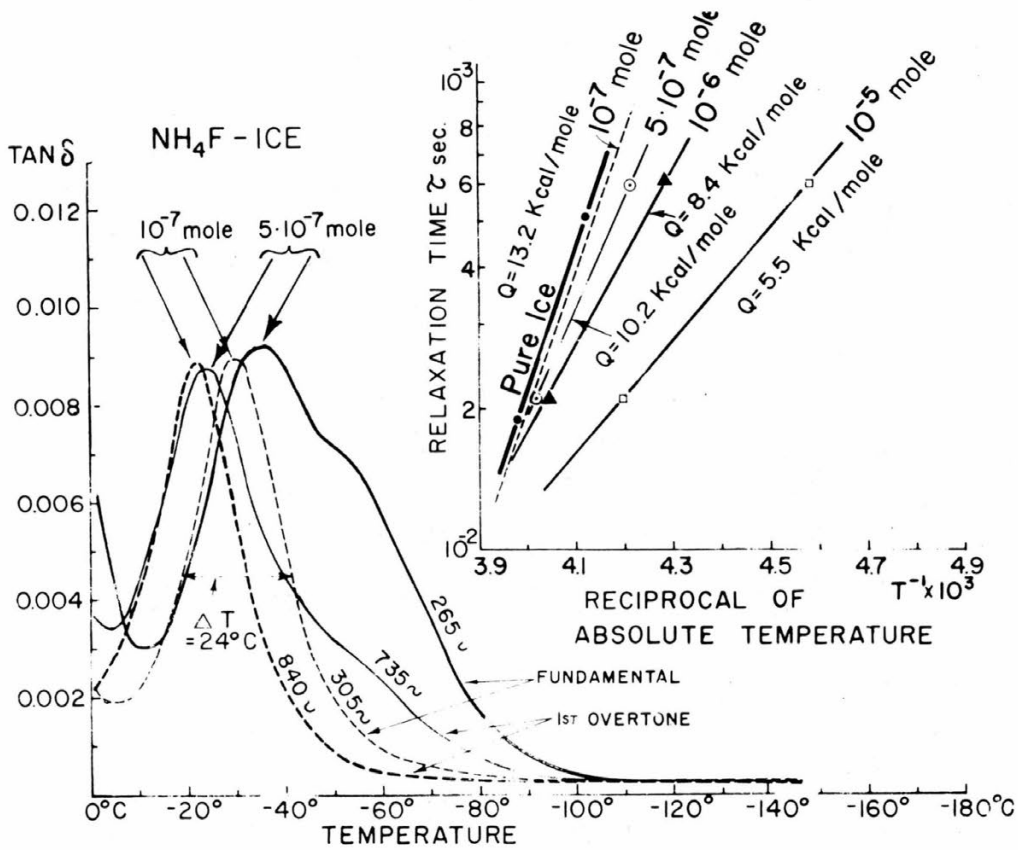

Figure 21. Effect of NH_4F concentration on damping.

Mechanical damping curves of artificially combined ice crystals

The curve in Figure 20C has been explained as a resultant of two kinds of relaxation curves, shown by m and n. A more concrete model concerning this problem can be demonstrated by use of artificially combined crystals. This experiment is not only useful in understanding the above-mentioned results, but it provides us with an important technique for the measurement of internal friction at individual grain boundaries.

A laboratory-made pure single crystal bar and a natural contaminated single crystal bar were welded at the center and trimmed by a microtome to the dimensions shown in Figure 22A. In Figure 22, P is the pure ice prepared in the laboratory, and Q is a natural contaminated single ice crystal. The electrical resistivity of the melted contaminated specimen was 450 Kohm·cm. The natural ice crystal was obtained from Lake Shikaribetsu, located in Hokkaido, Japan. As the lake ice consisted of fairly large grains (approximately 3 to 4 cm in diameter, 40 or 50 cm long), a single ice crystal bar was easily cut from one grain. Two dashed lines, P and Q, show the relaxation curves which would be obtained if the 172 mm long specimen was composed independently of a pure or of a contaminated single ice crystal. The damping maxima of the pure and contaminated ice are located at -32C and -63C, respectively. The height of maximum damping of Lake Shikaribetsu's ice was remarkably lower than that of the artificially made crystal because of the orientation of its c-axis (discussed below). In Figure 22A, a thick and a thin solid curve represent the resultant mechanical damping of this combined crystal measured at the fundamental (320 cps) and the first harmonic (890 cps) vibrations, respectively.

Another specimen was prepared in which the pure and the contaminated ice crystals were welded with a broad contact area, and then trimmed to the dimensions illustrated

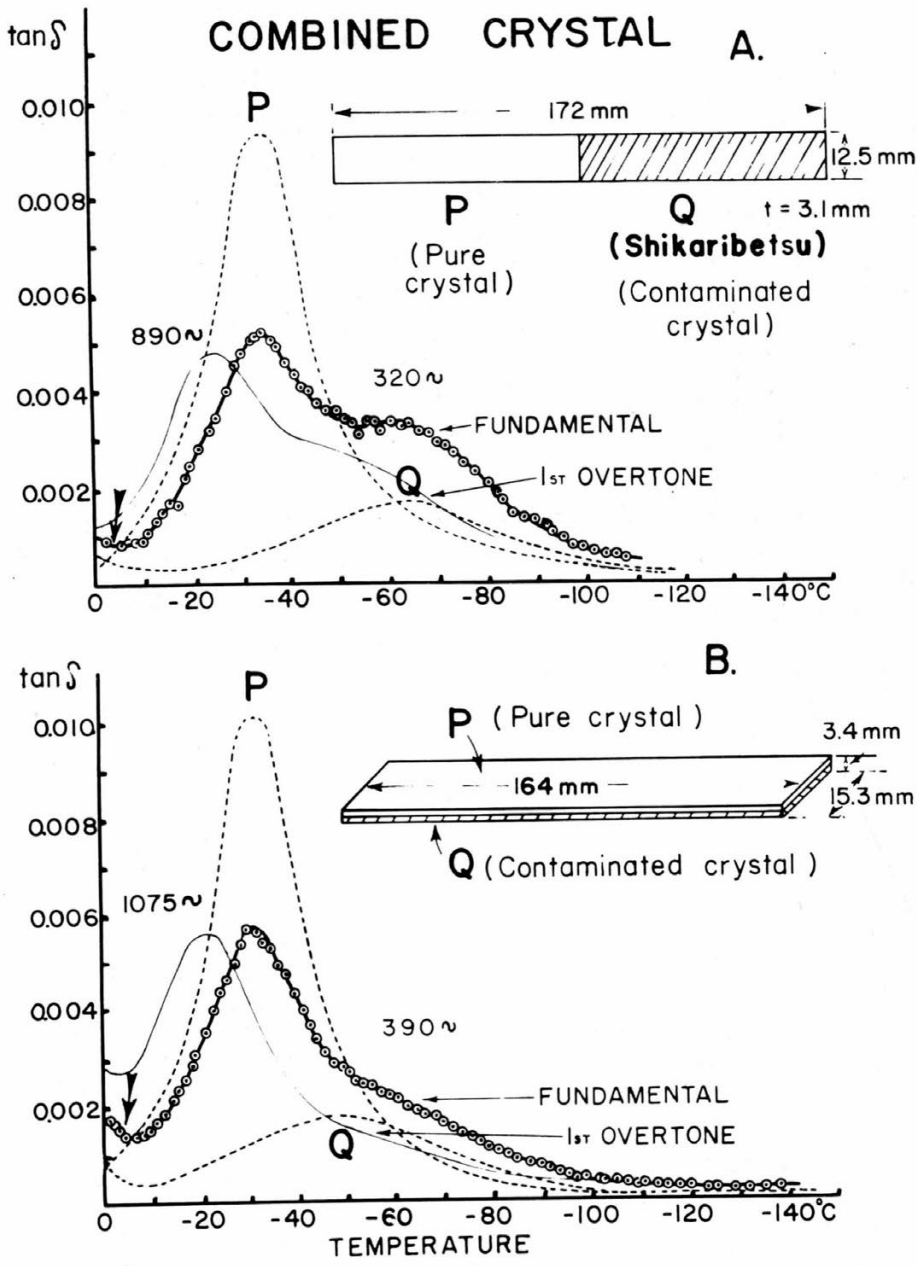

Figure 22. Mechanical damping of a combined crystal of pure and contaminated ice.

in Figure 22B. The resultant mechanical damping obtained at the fundamental and first harmonic vibrations are shown by thick and thin solid curves, respectively.

These curves are quite similar to the final stage of annealing in the NH_4F-doped specimen (Fig. 20C). The contaminated and the pure crystals exhibit their individual damping in the lower and higher temperature range, respectively.

Anisotropy of the height of maximum damping due to crystallographic orientation

In our experiments, the height of maximum damping due to proton movement in randomly oriented polycrystalline ice was between 0.0105 and 0.0080 (mean 0.0090)

in the frequency ranges of 170 to 2200 cps. Most specimens of pure or dirty ice showed a slight decrease in the height of maximum damping with increasing frequency. Since the crystals have a hexagonal structure, an important problem remains in determining the relation between height of maximum damping due to proton movement and c-axis orientation. P. Schiller (1958) found that maximum damping was six times higher in specimens with c-axis perpendicular to the direction of longitudinal oscillation than in specimens with c-axis parallel to oscillation. A similar relationship between maximum damping and crystallographic orientation was also revealed in our experiments by the flexural vibration.

Three different specimens of single crystal ice having different orientations were prepared (Fig. 23). Specimens A and B were cut from the same slightly contaminated ice crystal made in the laboratory. C was prepared from a natural single crystal of ice obtained from Lake Shikaribetsu. When specimens A and B were set in flexural vibration, the basal planes of A and the c-axis of B were perpendicular to each neutral plane. In specimen C, the c-axis was parallel to the neutral axis through the bar. In Figure 23, curves a and b show the mechanical damping of specimens A and B obtained at the fundamental frequency. No difference was observed in the height of the maxima, but appreciable difference was found in damping at low temperatures due to chemical impurities (indicated by arrow, Fig. 23). In the upper right corner of Figure 23 this difference is illustrated with an ordinate enlargement of five. Curve c represents the maximum damping of specimen C, showing one-fifth the value of A or B. When a specimen was prepared from the same Lake Shikaribetsu ice sample so that the direction of the c-axis was perpendicular to the neutral plane as in B, the height of its maximum damping coincided with B.

Influence of plastic deformation on maximum damping. In order to examine the effect of plastic deformation, specimen C was bent at -25C by supporting it at both ends and loading it at the center. After 2 days, the center of the ice bar was depressed about 15 mm. Then the specimen was turned over and reloaded at the center until the ice bar was straightened. The mechanical damping was measured again, but no change in the height of maximum damping was observed, implying that these deformations did not have any influence on the proton movement. Another specimen was prepared from a previously deformed single crystal and compared with a nondeformed specimen. Again, no difference was observed between the two damping maxima suggesting that plastic deformation cannot change the total number of lattice defects.

Conclusions

The internal friction of ice was measured by the flexural vibration method between 0C and -180C. In pure H_2O and D_2O ice, observed mechanical relaxation curves were narrow and sharp, and appeared in the high temperature range. Activation energy Q and the pre-exponential factor τ_0 agreed with those obtained by the dielectric relaxation method, implying that anelasticity in ice crystals is attributable to proton movement at lattice defects.

Contaminated ice crystals were made with various kinds of chemical additives. In doped ice crystals, the relaxation curves became broad and maximum damping appeared at temperature ranges lower than for pure ice. The observed relaxation time also shortened and the activation energy was half the pure ice value, implying that chemical impurities produce a great many lattice defects which contribute to proton movement. In NaCl-doped ice crystals, mechanical damping was affected in specimens made from solutions having concentrations above $5(10)^{-5}$ mole. In NH_4F-doped ice crystals, however, the lowest concentration that had an effect on mechanical damping was between 10^{-7} mole and $5(10)^{-7}$ mole.

Anisotropy of the height of maximum damping was investigated. The height of maximum damping of the specimens with their c-axis parallel to the neutral line of flexural vibration decreased to one-fifth that of the specimen with the c-axis perpendicular to the neutral line.

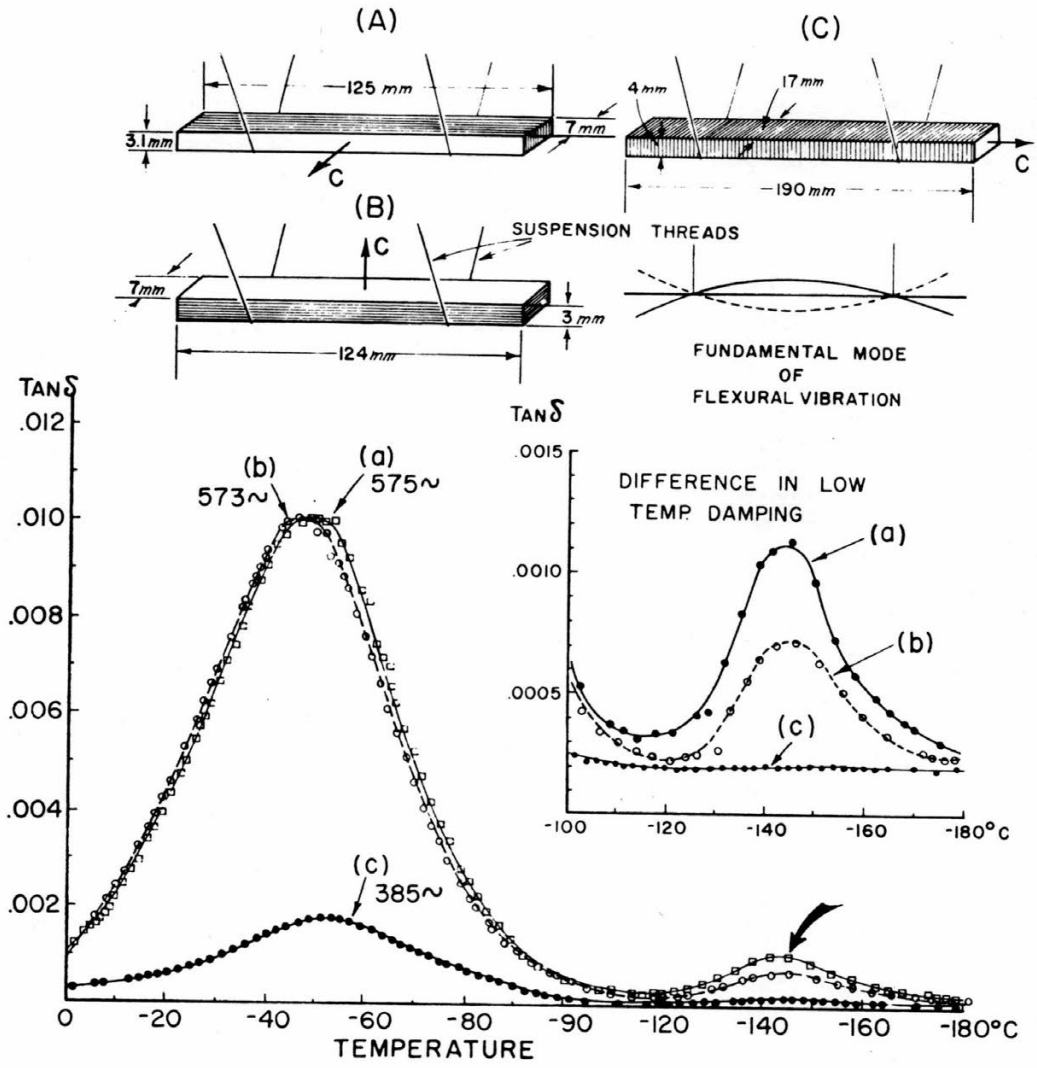

Figure 23. Anisotropy of height of maximum damping due to crystallographic orientation.

Another kind of damping, caused by chemical impurities concentrated in an aggregate form within the crystal lattice, was observed in the low temperature range (around -145C). The behavior of this damping is quite different from the anelasticity due to proton movement. The height of damping in this range was reduced with an increase of frequency and also by heat treatment. This damping probably was caused by oscillation of impurities occluded at localized imperfections such as microscopic holes or vacant places in the ice crystal lattice.

PART II. INTERNAL FRICTION AT CRYSTAL BOUNDARIES

Introduction

When the internal friction of polycrystalline ice was measured as a function of temperature, it was observed that the internal friction (tan δ) decreased very rapidly from high values near the melting point to very low values with a decrease in the temperature and then increased again toward a maximum value due to proton movement. There is no doubt that the steeply rising values for tan δ in the temperature range between -30 and 0C are caused by the grain boundaries, because this has never been observed in single crystal ice.

In our experiment with NaCl-doped ice crystals the steep grain boundary curve shifted toward the high temperature range with an increase in frequency (Fig. 8), and toward the low temperature range with an increase in NaCl concentration (Fig. 15). The dependence of grain-boundary internal friction on frequency and impurity concentration implies that it is produced by grain boundary viscosity, as found in polycrystalline metals by Kê (1947). It is also known that chemical impurities will concentrate at the grain boundaries rather than inside individual grains, with the amount of concentration varying from boundary to boundary. In contaminated polycrystalline ice, therefore, every grain boundary will have a different value of tan δ. The purpose of this investigation was to determine what mechanism is responsible for grain-boundary internal friction. The results indicate that the grain-boundary internal friction of polycrystalline ice is not always proportional to the total area of the crystal boundaries involved and that concentrated chemical impurities play an important role in grain boundary viscosity.

Internal Friction of Welded Boundaries

In an experiment described in Part I (Fig. 22), two combined crystals were made by welding pure and contaminated single-crystal specimens together at the melting point so that one combined crystal had a narrow welded interface and the other a broad interface. Since the crystallographic orientation was quite different in the two parts the welded interface can be considered to be an artificial grain boundary. The total interface areas of these two combined crystals are estimated from their dimensions to be 38.8 mm^2 for the narrow interface (A) and 2510 mm^2 for the broad interface (B). If a grain boundary always causes internal friction in the high temperature ranges between 0 and -30C, a steep variation of tan δ should be observed at the artificial grain boundaries in the combined crystals. Contrary to this assumption, the experimental data showed that the welded area produced no internal friction, although a small rise of the resultant internal friction, shown by a thick arrow in Figure 22, can be attributed to the contaminated crystal. If this rise had originated at the welded boundary, a high value of tan δ should have been observed in specimen B, because the total welded area of B is about 65 times larger than that of A.

It is interesting to note that the welded boundary between two crystals does not produce any internal friction in the frequency ranges used. (An explanation is given in the next section.)

Internal Friction at Individual Crystal Boundaries

A square ice plate (2 x 2 cm) containing a Y-shaped grain boundary was cut from a block of commercial ice. Two rectangular single crystal ice bars were welded to each side of this square ice plate. Then it was trimmed with a microtome to 185 x 15 x 2.7 mm. Figure 24, center, shows this "inlaid" grain boundary photographed under crossed polaroids; a-b and c-d are welded boundaries between the square ice plate and single crystal plates, and p-q and r-s form a Y-shaped crystal boundary. To show relative crystallographic orientations of both crystal and welded boundaries, evaporation etch pits were produced by a technique of Formvar film developed by Higuchi (1958). The specimen was placed in a cold box and the internal friction was measured by the flexural vibration method as described in Part I. The fundamental frequency was 240 cps. In Figure 25 curve A depicts the internal friction of the specimen with inlaid Y-shaped

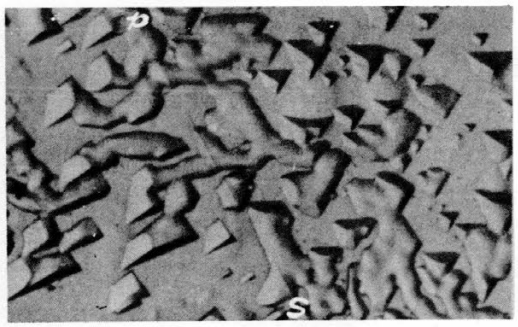

A. Etch pits along p-s.

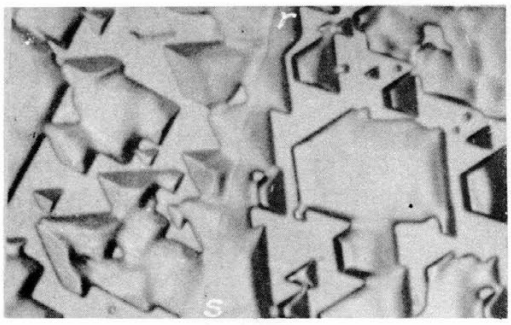

B. Etch pits along r-s.

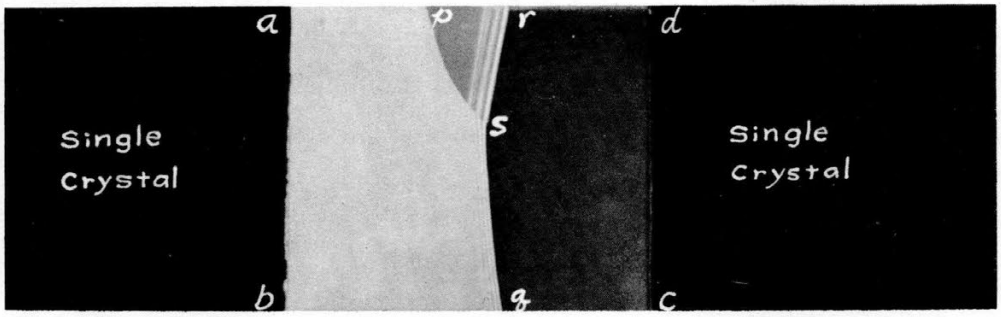

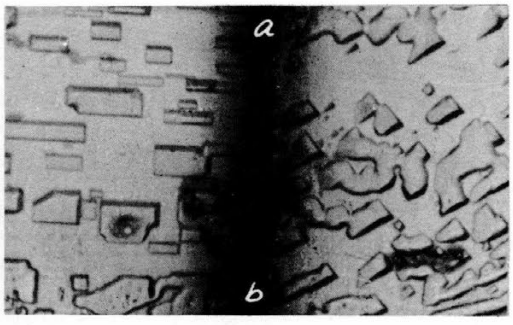

C. Etch pits along a-b.

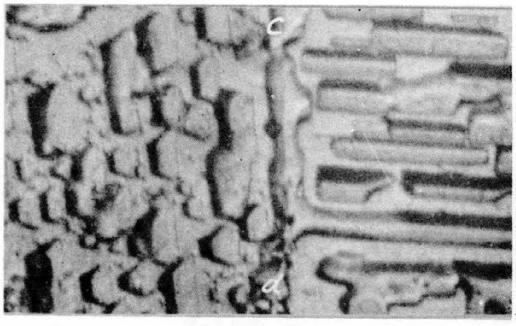

D. Etch pits along c-d.

Figure 24. Inlaid Y-shaped grain boundaries.

crystal boundaries, (A)'. A steep rise in tan δ is seen near the melting point. This can be attributed to the Y-shaped crystal boundaries, because, as noted above, this internal friction is not produced at welded interfaces.

A linear grain boundary was cut from the same block of commercial ice and inserted between two single crystal ice bars in the same manner as shown in Figure 25, specimen (B)'. The specimen was trimmed so that it would have approximately the same frequency as specimen (A)'. The grain boundary internal friction of this specimen (Fig. 25, curve B) shows a greater damping than that of the Y-shaped boundaries. A new grain boundary was inlaid in the same specimen as shown in Figure 25(C)'. Curve C shows the increase of tan δ due to the additional crystal boundary. Figure 26 shows the inlaid single linear boundary and the two inlaid crystal boundaries under polarized light.

Curve D in Figure 25 represents the steep rise of tan δ for an ice bar cut from ordinary commercial ice composed of many small grains (D)'. The average grain size

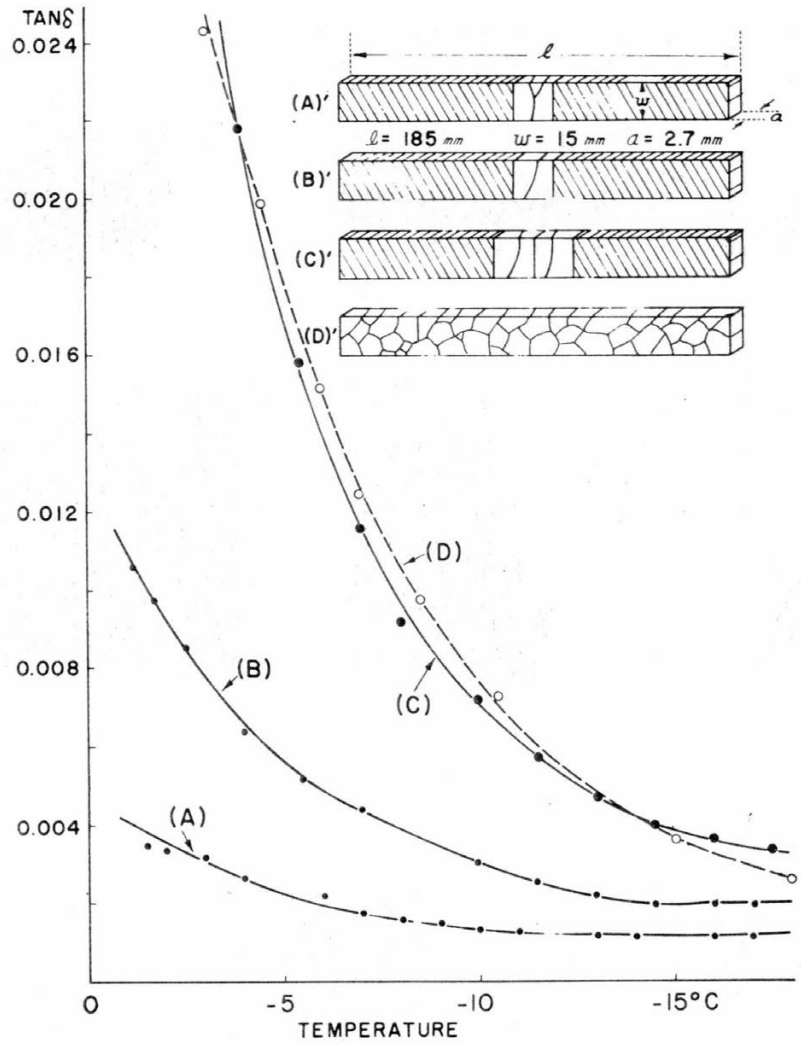

Figure 25. Mechanical damping of ice specimens with inlaid crystal boundaries. Fundamental mode (240 cps).

was 7 to 10 mm. No remarkable difference is observed between curves C and D, although the total area of the crystal boundaries of (D)' is very much greater than that of (C)'. Hence it appears that grain-boundary internal friction in contaminated polycrystalline ice is not always proportional to the total area of crystal boundaries, but depends upon the concentration of chemical impurities, which may differ from boundary to boundary.

Further confirmation of this inference was obtained by the following experiment. Two distinctly different crystal boundaries were obtained, one from a pure ice specimen and the other from an NaCl-doped ice crystal. The NaCl-doped ice crystal was grown from a 0.001-mole solution. Each ice block was inlaid and welded between two single crystal ice bars (Fig. 27). The bars were then trimmed to the same dimensions, so that they would produce equal frequencies. The structure of the pure ice crystal boundaries is much more complicated than that of the NaCl-doped boundaries.

Figure 28 shows the grain-boundary internal friction of both specimens measured at fundamental vibration (305 cps). Clearly the crystal boundaries containing NaCl have a higher internal friction than boundaries free of chemical impurity.

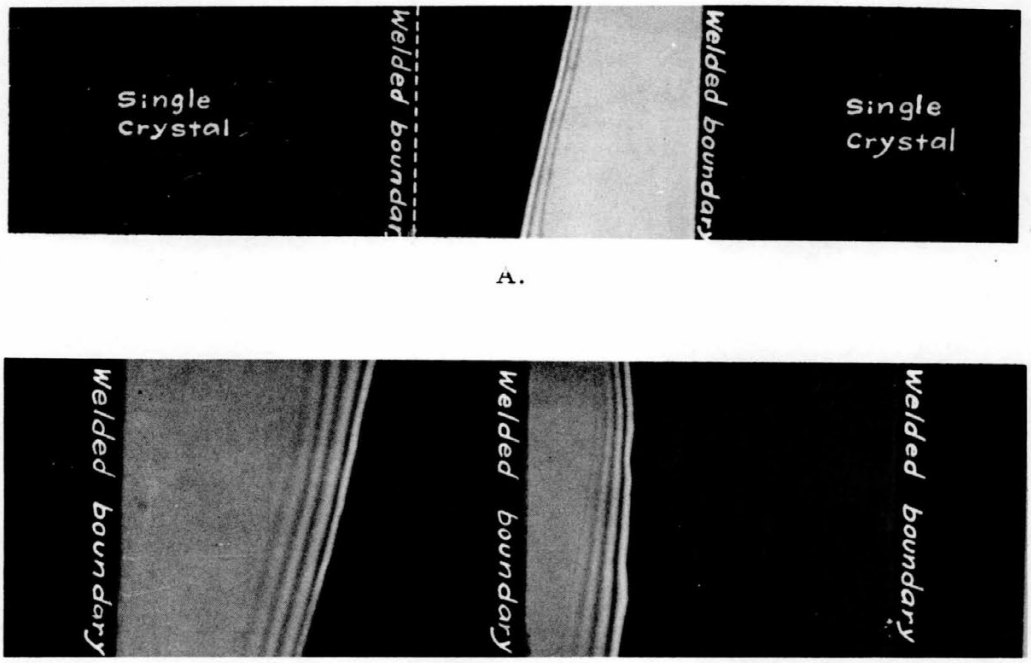

Figure 26. Inlaid linear crystal boundaries.

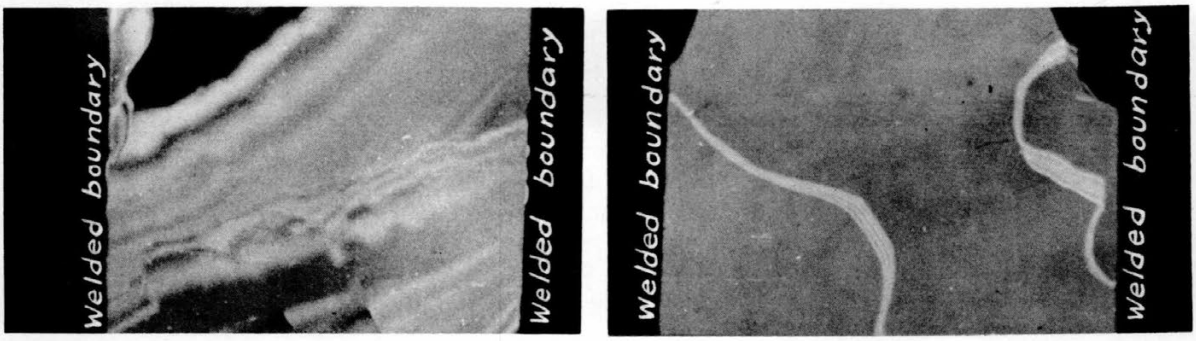

Figure 27. Inlaid crystal boundaries from pure ice (A) and NaCl-doped ice (B). (A) shows much more complicated structure than (B).

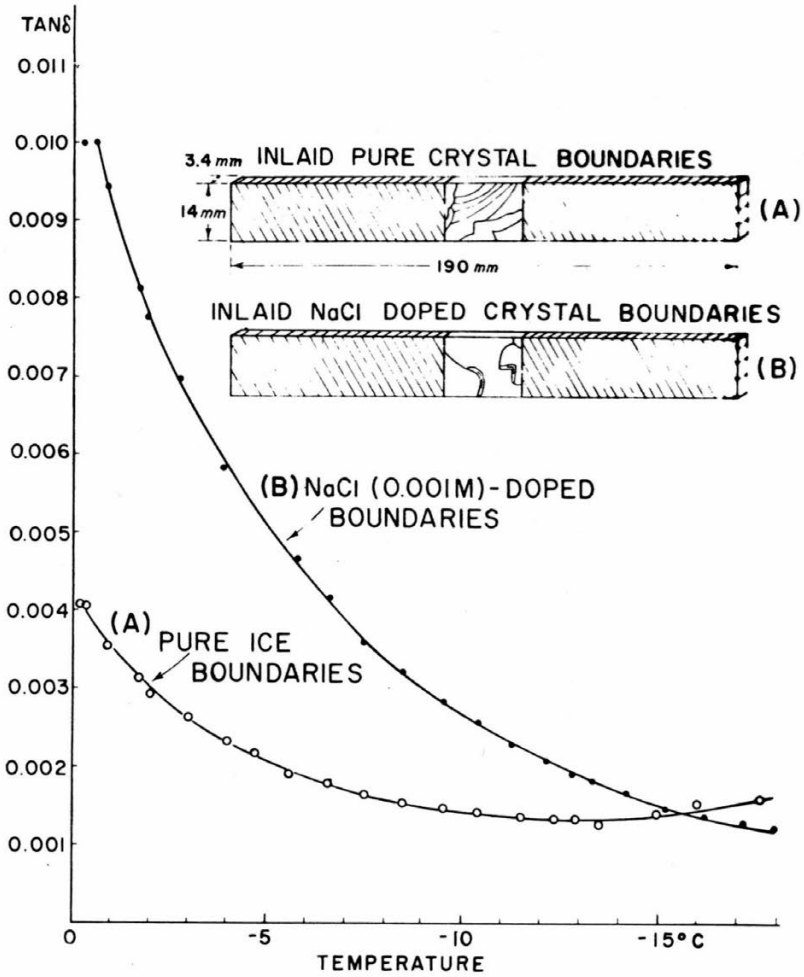

Figure 28. Grain-boundary internal friction in pure and NaCl ice. Fundamental mode (305 cps).

According to Kê (1947), grain boundary internal friction in polycrystalline metals is produced by "grain boundary viscosity". It is reasonable to expect that a concentration of chemical impurities would lower the freezing temperature, producing a thin liquid-like film at crystal boundaries. Therefore, it can be considered that the steep rise of tan δ near the melting point in polycrystalline ice is caused by a viscous layer at grain boundaries. This explains the fact that the artificially welded grain boundary interface of two crystals shows no appreciable internal friction. When two crystals are welded together at the melting point, melted water is squeezed out of the welded interface by compression, leaving no chemical impurities.

Activation Energy for Grain Boundary Viscosity

If we assume that the grain-boundary internal friction in an ice crystal is caused by anelasticity due to grain boundary viscosity, a steeply rising curve near the melting point should exhibit a well defined maximum. The location of the maximum should move toward the high temperature range with an increase in frequency, and the dispersion of resonant frequency should also occur in the same temperature range. In our experiments, however, no maximum damping was observed in the high temperature range, although the steep rise of tan δ appeared, showing a temperature shift with frequency. The main reason why it was impossible to observe maximum damping was the high frequency used.

The observed steep curves of tan δ, therefore, can be considered to be slopes coming down from "hidden maxima". In order to observe the complete shape of the grain-boundary internal friction damping maximum, the measuring frequency must be lowered as much as possible.

If the following approximation is permitted, we can estimate roughly the activation energy for grain boundary viscosity. Figure 29A depicts grain-boundary internal friction observed in NaCl-doped ice crystallized in a 0.001-mole solution. The curves show parallel displacement toward the high temperature range with increasing frequency. A horizontal line cutting all of the slopes at a point where they are parallel provides a means of determining the absolute temperature difference between any two slopes. This temperature difference is then assumed to be the same as the temperature difference between the maxima of these slopes. On this assumption, the linear relationship between the reciprocal of these absolute temperatures and their related frequencies (Fig. 29B) gives an estimate of activation energy. A horizontal line was drawn at tan δ = 0.010 at which point it cut the four curves at -7.8C, -5.6C, -3.2C and -1.0C, respectively. The resulting activation energy equals approximately 30.9 Kcal/mole.

The same procedures were applied to many specimens of pure and doped ice crystals in order to obtain the activation energy for grain boundary viscosity. The results are:

Pure H_2O ice	74.5 Kcal/mole	
	57.5 Kcal/mole	
D_2O ice	55.9 Kcal/mole	
	57.5 Kcal/mole	
NaCl-doped ice	0.005 mole	30.9 Kcal/mole
	0.001 mole	30.6 Kcal/mole
	0.0005 mole	42.0 Kcal/mole
	0.00005 mole	51.6 Kcal/mole
	0.00001 mole	59.2 Kcal/mole
HCl-doped ice	0.002 mole	36.0 Kcal/mole
Commercial ice	32.0 Kcal/mole	(average of 5 samples)
HF-doped ice	0.0025 mole	59.0 Kcal/mole.

Inspection of these data shows that the activation energy for grain boundary viscosity of pure H_2O and D_2O ice is approximately twice as high as that of NaCl-, HCl-doped ice crystals, or commercial ice. In NaCl ice crystals, the activation energy decreased with an increase in concentration. The activation energy for HF-doped ice was the same as the value for pure ice. Since these data were obtained through a procedure which is based on an assumption, the data may deserve re-examination in future studies concerning this problem.

Conclusions

The grain-boundary internal friction was measured by cutting an individual crystal boundary from polycrystalline ice and then inlaying it into a single crystal bar. It was confirmed that grain-boundary internal friction differs from boundary to boundary, and is not always proportional to the total area of the boundaries, but depends upon concentrated chemical impurities.

The activation energy for grain boundary viscosity was estimated assuming that the shift of the observed curves of tan δ toward the high temperature range with increasing frequency is due to anelasticity at grain boundaries. The estimated values for the activation energy were roughly 60 Kcal/mole for pure ice and 30 Kcal/mole for doped ice.

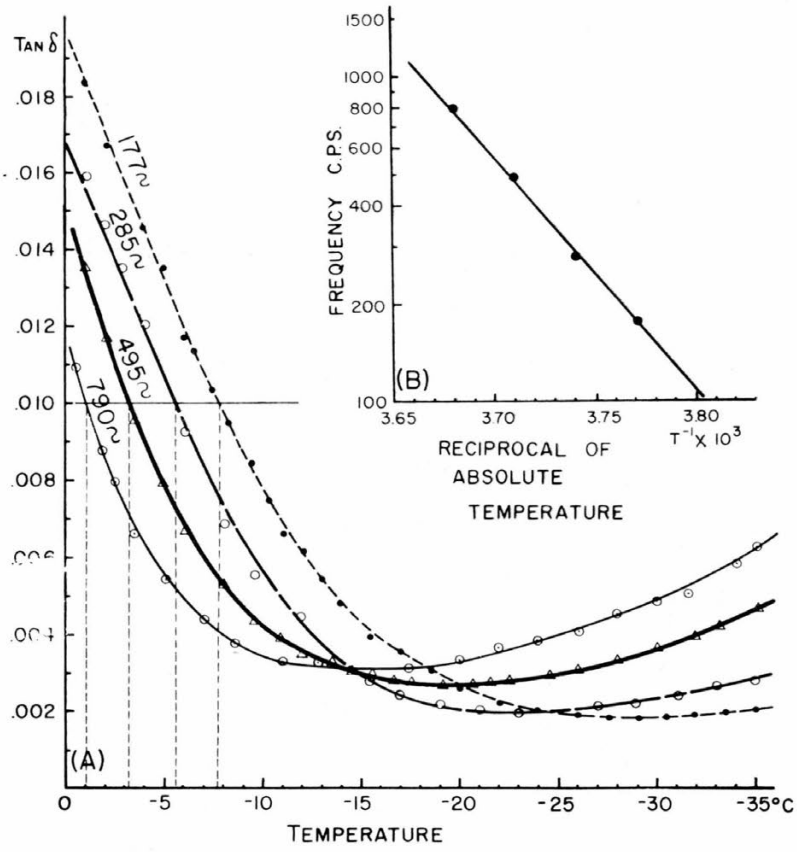

Figure 29. Estimation of activation energy for grain boundary viscosity, NaCl ice.

PART III. THE INTERNAL FRICTION OF NATURAL GLACIER ICE

Introduction

The formation of natural glacier ice is quite different from the formation of ordinary ice crystals grown from a melt. The ice of high polar glaciers is formed through densification of snow without ever being subjected to thawing. Snow crystals grow by sublimation of water vapor around tiny particles suspended in the air; while falling through the lower atmosphere the crystal surfaces become contaminated with impurities. The main sources of the chemical impurities found in glacier ice are the nuclei around which the snow crystals originally developed and the atmospheric aerosols captured by the snowflakes while falling to the ground. A very interesting problem arises as to how the impurities are distributed within glacier ice and how they influence mechanical damping. Since the International Geophysical Year, the author has had many chances to study the internal friction of glacier ice from Greenland, Antarctica, and Le Conte Glacier (west coast of Canada). Their characteristic internal friction curves are well explained by the experimental results given in the preceding two parts.

Temperature Dependence of Internal Friction in Ordinary Polycrystalline Ice

Figure 30A (solid curves) depicts a typical temperature dependence of the internal friction (tan δ) of contaminated polycrystalline ice. Three remarkable variations in tan δ are seen in the temperature range between 0C and -180C as indicated by G, P, and I. Both P and G shift toward the high temperature range with an increase in the frequency, implying that they are caused by anelasticity due to proton movement and grain

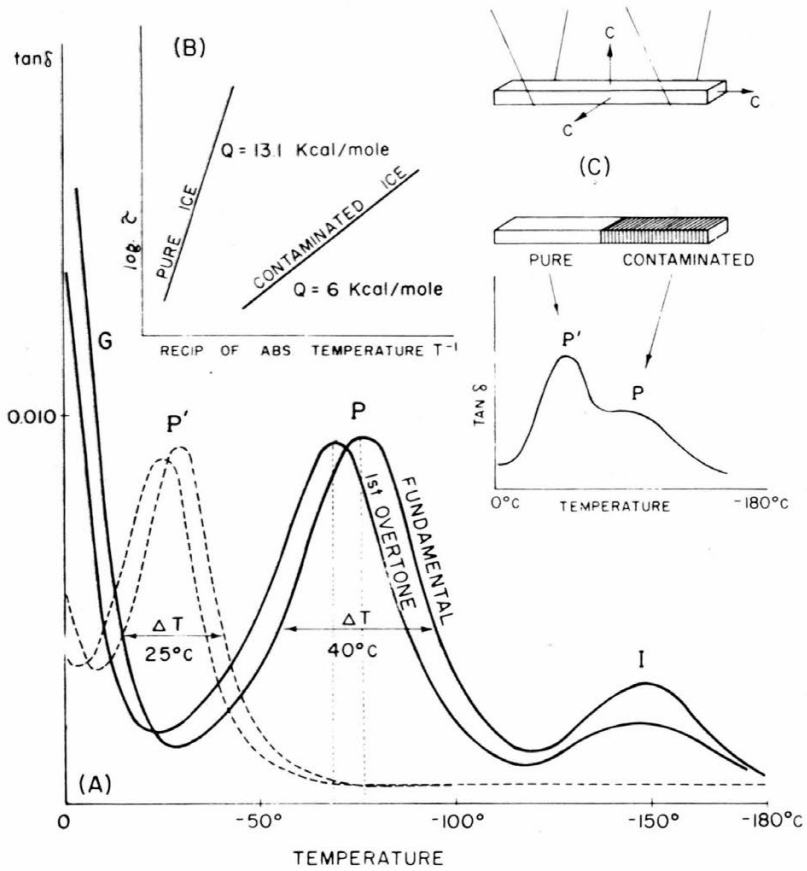

Figure 30. Typical temperature dependence of internal friction of contaminated ice (solid line) and pure ice (dashed line).

boundary viscosity, respectively. The mound-like damping, observed only in contaminated specimens, decreases with an increase of the frequency and with long-time annealing, suggesting that this damping is produced by chemical impurities trapped locally within grains in an aggregated state. The relaxation curve of pure ice P' appears in a higher temperature range than contaminated ice, with a narrow width ΔT (the temperature interval at one-half the height of the damping maximum) = 25C. In the contaminated ice ΔT is approximately 40C. This broadness is due to chemical impurities trapped in the ice crystal lattice.

When the logarithm of relaxation time τ (inverse of angular frequency at maximum damping) is plotted against the reciprocal of the absolute temperatures at which maximum damping occurs, the curve for pure ice appears in the high temperature range with a steep slope. Its activation energy is Q = 13.1 Kcal/mole. The curve for contaminated ice appears in the low temperature range with a low slope, having an activation energy of Q = 6 Kcal/mole, as illustrated in Figure 30B.

Artificially combined crystals made by welding together both pure and NH_4F contaminated ice bars showed a bimodal curve which consists of a superposition of P and P' as depicted in Figure 30C. Hence, if a bimodal relaxation curve is observed in some specimen, it can be concluded that the specimen may be composed of two component crystals which differ from each other in impurity content.

Investigation of a single ice crystal having different crystallographic orientations showed that the height of maximum damping of the specimens having c-axis parallel

to the neutral line of the flexural vibration decreases to one-fifth of that of the specimen in which the c-axis was perpendicular to the neutral line.

These experimental facts provide very useful data for interpretation of the characteristic damping curve of natural glacier ice.

Experimental Results

Internal friction of Greenland glacier ice

These ice samples were obtained from an ice tunnel (1167 ft long) excavated on the edge of the Ice Cap at Tuto about 15 miles east of Thule, Greenland. All specimens were removed carefully from the ice wall with the aid of a CRREL 3-in. diam coring auger. According to Butkovich (1959), five types of ice were identified by differences in color, grain size, size and shape of entrapped air bubbles, and c-axis orientation. The internal friction of two specimens was studied.

Figure 31 illustrates the internal friction of an ice sample obtained from active glacier ice located 264 ft from the portal of the ice tunnel. The average grain size of the specimen was 7 mm and it contained elongated and aligned air bubbles. Its density was 0.905 and the electrical resistivity of the melted sample was 400 Kohm·cm. Butkovich (1959) states that the c-axes of this specimen are randomly oriented, as shown in the Schmidt diagram in Figure 31. Two rectangular ice bars were cut from this ice core, parallel to the cylinder axis, and trimmed to 173 x 19 x 5 mm and 182 x 18 x 3 mm. Internal friction was measured at the fundamental and the first overtone oscillations. Resonant frequencies at maximum damping are indicated on each curve. Both the steep rise of tan δ due to the grain boundaries and broad relaxation curves modified by impurities were observed, but no mound-like damping appeared in the low temperature range as was observed in ice crystals grown from a melt.

Figure 32 shows the internal friction of an ice specimen obtained 650 ft from the portal of the ice tunnel. The average grain size of this sample was 5 mm in diameter. It contained homogeneously distributed spherical air bubbles less than 1 mm in diameter and also fine silt bands. Its density was 0.912 and the electrical resistivity of the melted sample was 185 Kohm·cm. Comparatively lower values for the electrical resistivity of this sample may be due to the silt bands. A petrofabric study of an ice plate cut perpendicular to the core axis indicated a strong polar orientation of the c-axis (Fig. 32). A rectangular bar was cut parallel to the core axis, and trimmed to 114 x 13 x 4 mm, consequently the c-axis and the bar axis are parallel. Lower values of maximum damping, due to crystallographic orientation, were observed as expected from the experimental data for single crystal ice. No mound-like damping in the low temperature range was observed in this sample, though a larger amount of chemical impurities was involved.

Plots of log τ vs T^{-1} are given in Figure 35, and the activation energy values are indicated. The values are quite similar to those of contaminated ice crystals grown from a melt.

The broadness of the relaxation curve, the low value of activation energy, and no mound-like damping around -145C imply that chemical impurities in glacier ice can exist within grains in the atomic state but not in aggregates. Almost all chemical impurities found in glacier ice may have been derived from the sublimation nuclei of snow crystals and secondary contamination due to atmospheric suspensions or aerosols. Since high polar glacier ice has never been subjected to melting, it is believed that these chemical impurities may have been incorporated within the ice crystal lattice through densification processes and long annealing under high pressure.

Internal friction of Antarctic iceberg ice

This sample was obtained from a grounded iceberg near Showa Base (39° 31'E, 69° 02'S), Antarctica. Although the true age of this iceberg is not known, it is supposed that it has been subjected to erosion by wind and melt water for a long time. Many aligned air bubbles and healing interfaces of thermal cracks were observed. The density was 0.86. The electrical resistivity of the melted sample was 230 Kohm·cm.

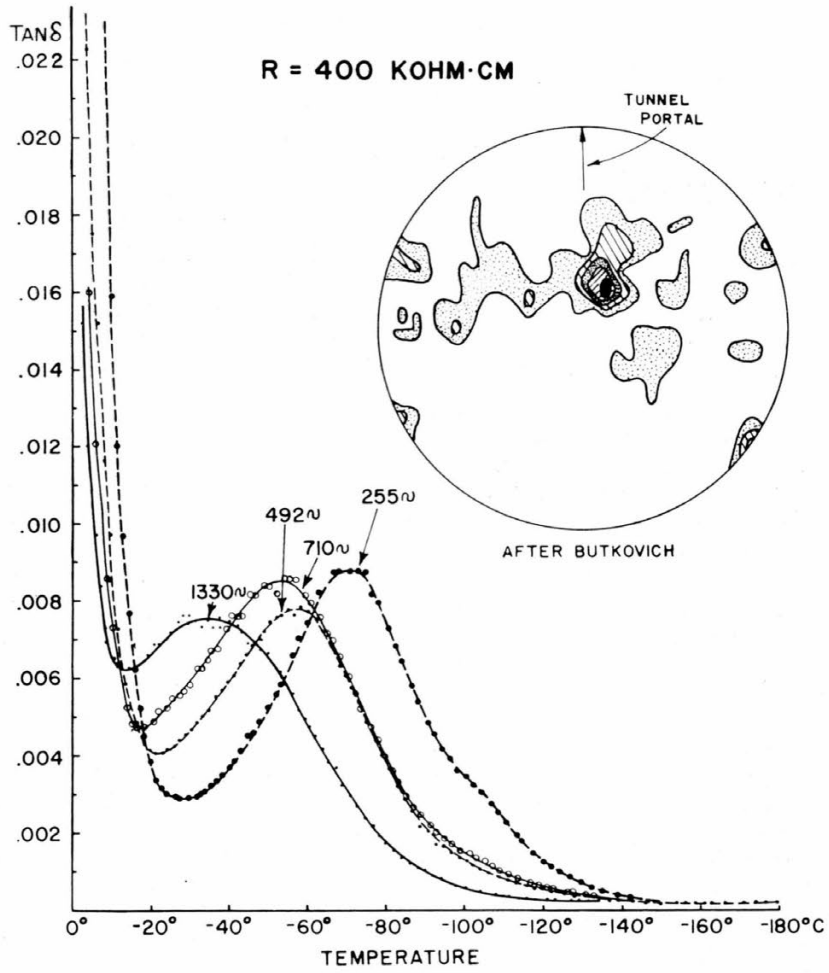

Figure 31. Internal friction of Greenland glacier ice, random orientation.

The internal friction of two specimens, one cut vertically and one horizontally from the same block of ice, is shown in Figure 33. The relaxation curves of both samples are very broad and have obvious shoulders on the low temperature side of the curves. These shoulders can be considered to be a resultant of the two imaginary curves depicted by dotted lines. In actuality, these dotted curves probably represent the internal friction of ice crystals containing different concentrations of chemical impurities, which may occur through repeated thawing and freezing during the summer season. The only justification for these assumptions is the experimental results obtained from a combined crystal composed of both pure and contaminated ice bars (Fig. 22). The combined crystals exhibited a bimodal curve which was made by the superposition of two relaxation curves.

Relaxation time of Antarctic iceberg ice vs T^{-1} is plotted in Figure 35.

Internal friction of Le Conte Glacier ice

Le Conte Glacier is located at 56° 45'N and 130° 30'W (west coast of Canada). The ice samples from this glacier were initially obtained by a Japanese crew who took aboard several floating ice blocks that had calved from the terminal portion of the glacier. Two kinds of ice were identified by differences in grain size, transparency, and entrapped air bubbles. One of them was transparent ice, containing no air bubbles

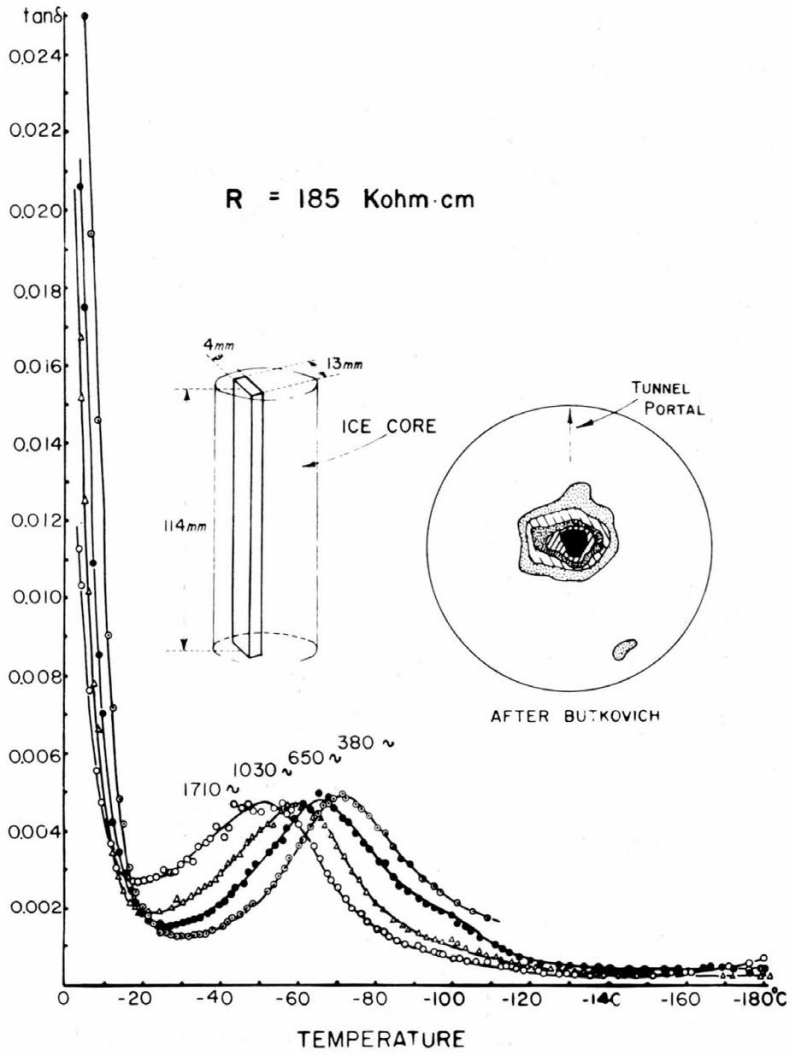

Figure 32. Internal friction of Greenland glacier ice, c-axis parallel to plane of vibration.

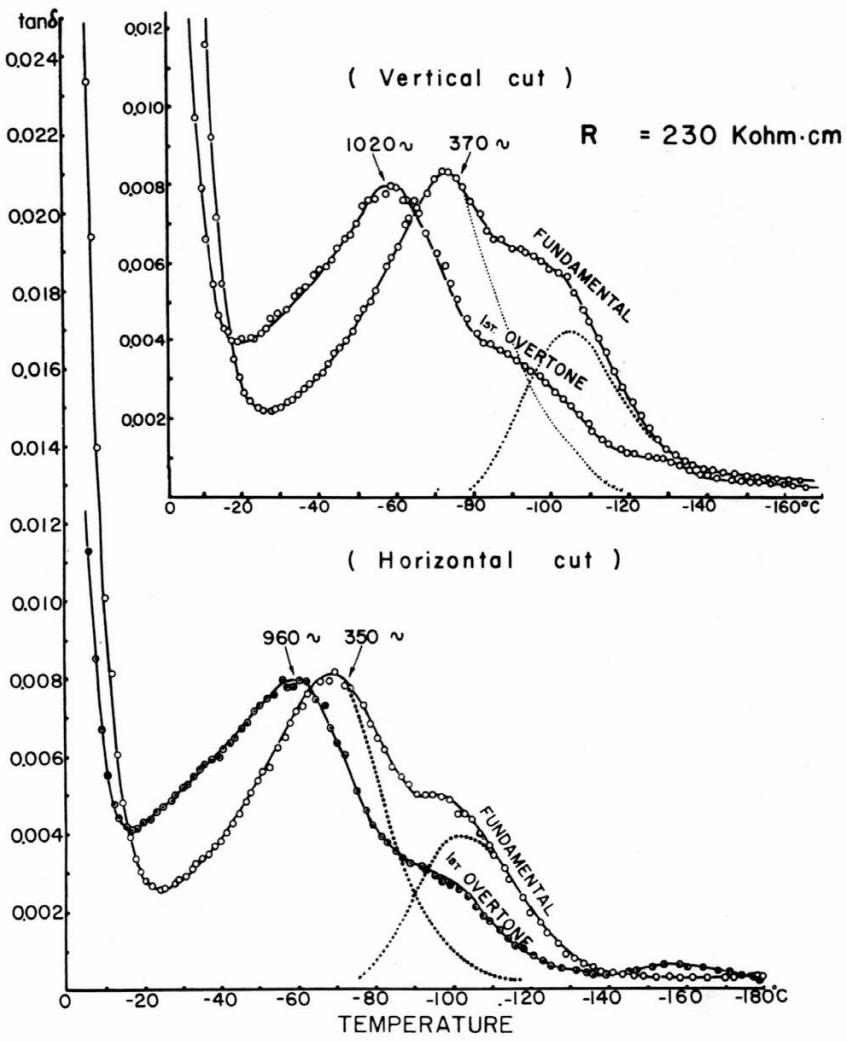

Figure 33. Internal friction of Antarctic iceberg ice.

and consisting of fairly large grains from 20 to 30 mm in diameter. The electrical resistivity of this melted specimen was 500 Kohm·cm. Another specimen consisted of opaque ice made up of many small grains containing tiny air bubbles. The electrical resistivity of this melted specimen was 700 Kohm·cm. It is not known how much time elapsed after these ice blocks calved into the sea, but there is no doubt that they have been subjected to annealing at the melting point for a long period of time. The internal friction curves for these specimens are illustrated in Figure 34.

A cursory glance at these figures will show that the relaxation curves of Le Conte Glacier ice are quite different from those of both Greenland and Antarctic glacier ice. The damping maxima (curves on the high temperature side are depicted by dotted lines) due to proton movement appear very close to the steep rise of tan δ produced at the grain boundaries. When the relaxation times of these specimens are plotted logarithmically against T^{-1}, they appear in the same temperature range as those of pure ice crystals (Fig. 35). The activation energy of Le Conte Glacier ice is equal to that of pure ice, even though it is contaminated with chemical impurities. (Glacier ice from Greenland and Antarctica or doped ice crystals have an activation energy of approximately

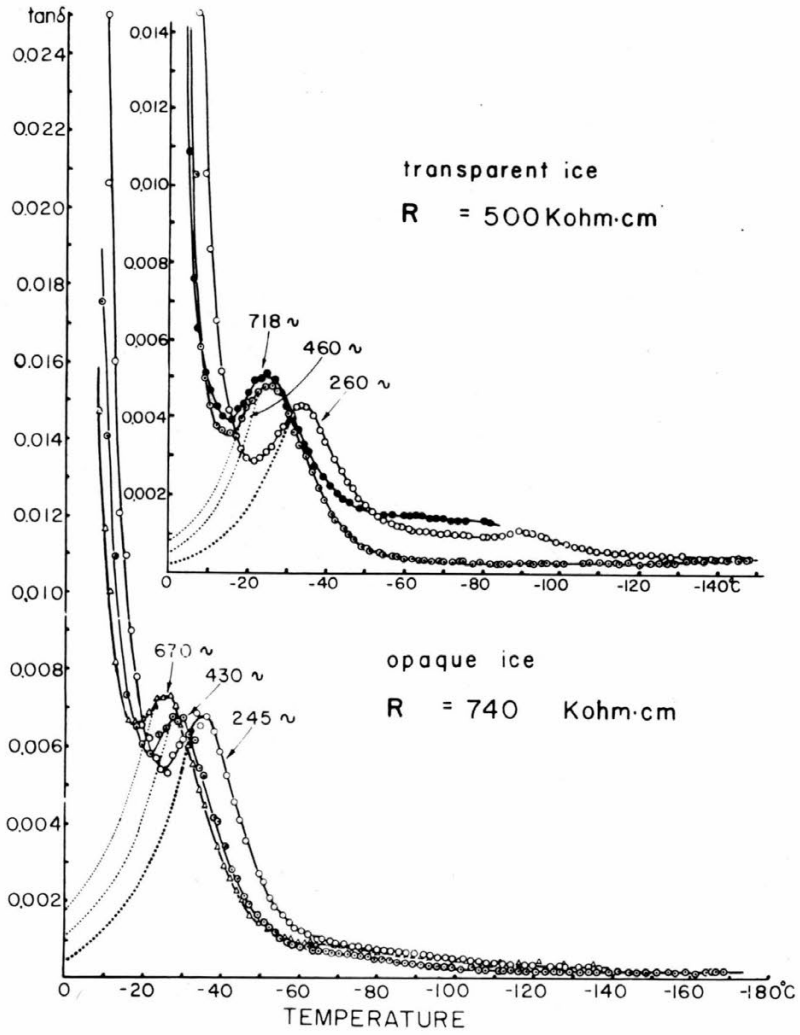

Figure 34. Internal friction of Le Conte Glacier ice (temperate glacier).

6 Kcal/mole.) This peculiar behavior of Le Conte Glacier ice can be explained if we recognize that almost all chemical impurities have diffused from within the grains to the grain boundaries, because of long annealing near the melting point.

Renaud André (1951) found that Z'Mutt Glacier (temperate glacier in Switzerland) consisted of pure ice grains surrounded by a concentrated saline film. After Renaud's experiment, the following examination was carried out. A specimen of Le Conte Glacier ice (transparent ice) was exposed to a strong infrared lamp. Separation of the grains occurred by rapid melting of the grain boundaries. A thin surficial layer from each grain was melted and collected in a glass bottle, then the center portions of the grains were melted in order to measure their electrical resistivities separately. The electrical resistivities of the melted grain boundaries and the center of the grains were found to be 88 Kohm·cm and 800 Kohm·cm, respectively. The lower resistivity at the grain boundaries is enough to substantiate the above statements.

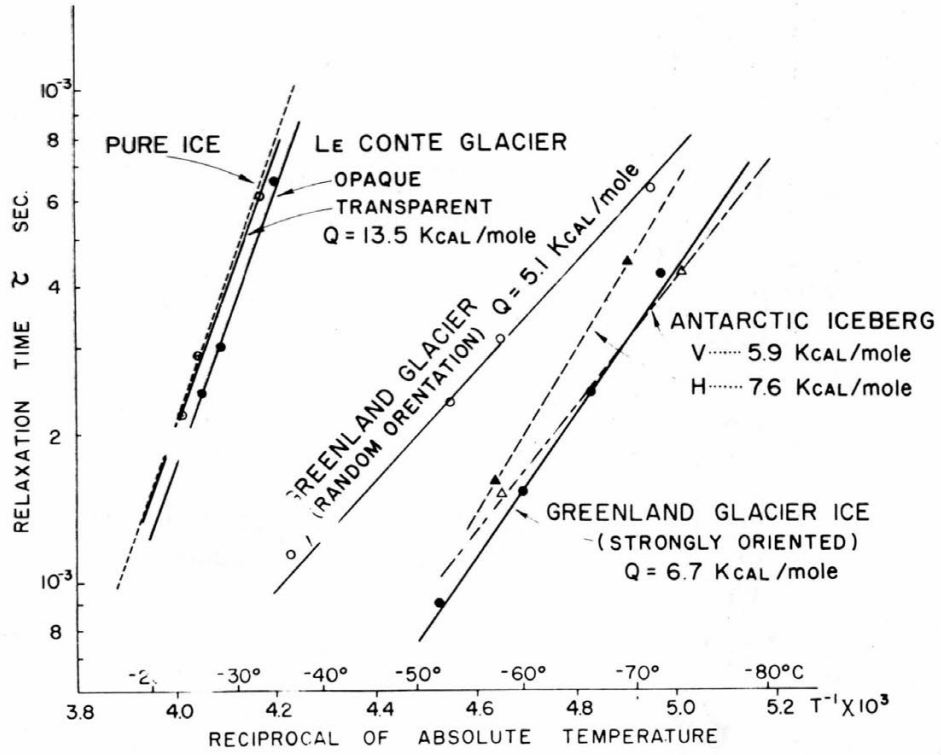

Figure 35. τ vs T^{-1} at maximum damping, natural glacier ice.

Activation Energy for Grain Boundary Viscosity of Glacier Ice

The activation energy for grain boundary viscosity of glacier ice was estimated by the approximate method used in Figure 29. The results are:

Greenland glacier ice — randomly oriented grains (R=400 Kohm·cm) 36.5 Kcal/mole
— strongly oriented grains (R=185 Kohm·cm) 38.0 Kcal/mole
Antarctic iceberg ice — horizontal cut specimen (R= 230 Kohm·cm) 34.0 Kcal/mole
— vertical cut specimen (R=230 Kohm·cm) 35.0 Kcal/mole
Le Conte Glacier ice — transparent, large grains (R=500 Kohm·cm) 36.0 Kcal/mole
— opaque, small grains (R=700 Kohm·cm) 35.0 Kcal/mole.

These values were quite similar to those obtained in commercial or contaminated polycrystalline ice.

Conclusions

Greenland glacier ice and ordinary ice grown from a melt exhibit similar relaxation curves. The broad relaxation curves of glacier ice indicate that some chemical impurities are incorporated into ice grains through the densification process of snow. The mound-like damping curve observed in ordinary ice around -145C has never been observed in glacier ice, suggesting that chemical impurities exist in an atomic state rather than in an aggregate state within the grains. Bimodal relaxation curves observed in Antarctic iceberg ice can be explained by assuming that the ice consists of two types of crystals containing different concentrations of chemical impurities which might develop through repeated thawing and freezing. The narrow relaxation curve found in Le Conte Glacier ice suggests that all chemical impurities have diffused from within the grains to the crystal boundaries during long annealing at the melting point. This is supported by the fact that the electrical resistivity of the melted boundary zone is much lower than that of the melted central portion of the grains.

REFERENCES

Auty, R. P. and Cole, R. H. (1952) Dielectric properties of ice and solid D_2O, Journal of Chemical Physics, vol. 20, p. 1309-1314.

Bjerrum, N. (1952) Structure and properties of ice, Science, vol. 115, p. 385-390.

Brill, R. and Camp, P. R. (1961) Properties of ice, U. S. Army Snow, Ice and Permafrost Research Establishment (USA SIPRE) Research Report 68.

Butkovich, T. R. (1959) Some physical properties of ice from the TUTO tunnel and ramp, Thule, Greenland, USA SIPRE Research Report 47.

Gränicher, H., Jaccard, C., Scherrer, P., and Steinemann, A. (1947) Dielectric relaxation and the electrical conductivity of ice crystals, Discussions of the Faraday Society, no. 23, p. 50-62.

Higuchi, K. (1958) The etching of ice crystals, Acta Metallurgica, vol. 6, p. 636-642.

Kê, T. S. (1947) Experimental evidence of the viscous behavior of grain boundaries in metals, Physical Review, vol. 71, p. 533-546.

Kingery, W. D. (1960) Regelation, surface diffusion, and ice sintering, Journal of Applied Physics, vol. 31, p. 833-838.

Kneser, H. O., Magun, S., and Ziegler, G. (1955) Mechanische Relaxation von einkristallinem Eis (Mechanical relaxation of monocrystalline ice, Naturwissenschaften, vol. 42, p. 437 (text in German).

Kuroiwa, D. (1961) A study of ice sintering, Tellus, vol. 13, no. 2, p. 252-259. Also U. S. Army Cold Regions Research and Engineering Laboratory (USA CRREL) Research Report 86, 1962.

_____ and Yamaji, K. (1956) 0°~-100°C no han-i ni okeru kori nentansei. I. (Visco-elastic property of ice in the temperature range 0°~-100°C. I, Teion Kagaku, Series A, vol. 18, p. 97-114 (text in Japanese).

_____ (1959) Takessho oyobi tankessho no kori no naibu masatsu (Internal friction of poly- and single-crystal ice), Teion Kagaku, Series A, vol. 18, p. 97-114 (text in Japanese).

Nakaya, U. (1956) Properties of a single crystal of ice, revealed by internal melting, USA SIPRE Research Report 13.

_____ (1959) Visco-elastic properties of processed snow, USA SIPRE Research Report 58.

Renaud, A. (1951) Nouvelle contribution à l'etude du grain de glacier (New contribution to the study of glacier particles), General Assembly of Brussels, International Union of Geodesy and Geophysics. International Association of Scientific Hydrology, vol. 1, p. 206-211 (text in French).

Schiller, P. (1958) Die mechanische Relaxation in reinen Eisenkristallen (Mechanical relaxation in pure singlecrystals of ice), Zeitschrift für Physik, vol. 153, p. 1-15 (text in German). National Research Council, Canada, Technical Translation TT-890.

Truby, F. K. (1952) A study of the electrical properties of ice, New Mexico Institute of Mining and Technology, Research and Development Division, Project NR-082-094, Report no. 2.

_____ (1955) Lattice constants of pure and fluoride-contaminated ice, Science, vol. 121, p. 404.

Zaromb, S. and Brill, R. (1956) Solid solutions of ice and NH_4F and their dielectric properties, Journal of Chemical Physics, vol. 24, p. 895-902.